Theoretical Feasibility of Cold Fusion According to the BSM - Supergravitation Unified Theory

Stoyan Sarg Sargoytchev
York University, Toronto, Canada *
E-mail: stoyans@yorku.ca

Advances in the field of cold fusion and the recent success of the nickel and hydrogen exothermal reaction, in which the energy release cannot be explained by a chemical process, need a deeper understanding of the nuclear reactions and, more particularly, the possibility for modification of the Coulomb barrier. The current theoretical understanding based on high temperature fusion does not offer an explanation for the cold fusion or LENR. The treatise "Basic Structures of Matter – Supergravitation Unified Theory", based on an alternative concept of the physical vacuum, provides an explanation from a new point of view by using derived three-dimensional structures of the atomic nuclei. For explanation of the nuclear energy, a hypothesis of a field micro-curvature around the superdense nucleus is suggested. Analysis of some successful cold fusion experiments resulted in practical considerations for modification of the Coulomb barrier. The analysis also predicts the possibility of another cold fusion reaction based on some similarity between the nuclear structures of Ni and Cr.

Keywords: cold fusion, LENR, Coulomb barrier, atomic nuclear structures, alpha decay

1. Introduction

The scientific research on cold fusion was pioneered by High Flyn (1913-1997), an emeritus professor at the University of Rochester. Being an expert in ultrasonic waves, he advocated a method of cold fusion based on cavitation in liquid metals with injected hydrogen or deuterium and obtained a patent in 1982 [1]. At this time however, little attention was paid since cold fusion was thought to be theoretically impossible. Interest in cold fusion was raised after Fleischmann and Pons announced a successful cold fusion experiment in 1989 [2]. The lack of a theoretical explanation and difficulty in repeatability led to an official denial, but interest in this option for solving the energy crisis never disappeared. Due to opposition from mainly the hot fusion advocates, the field is more often referred to as Low Energy Nuclear Reaction (LENR). Many researchers and scientists around the world have reported successful experiments at a number of international conferences [3], and selected articles are collected in an on-line data base [4]. The results, however, have not been taken seriously by main stream science, even after full support by two Nobel laureates, Julian Schwinger and Brian Josephson. Julian Schwinger (1918-1994), a Nobel prize winner in Physics, 1965, who also worked with Oppenheimer, was a strong advocate of cold fusion [5]. Brian Josephson, a Nobel prize winner in Physics, 1973, is a discoverer of the Josephon effect in the field of superconductivity. He is presently a strong supporter of cold fusion [6]. The reported successful experiments from many laboratories around the world (now over 60), however, attracted attention. At the Tenth International conference on cold fusion, 2003, Cambridge, MA, T. O. Parcel summarized the results of four years of effort in a well equipped government laboratory to find an explanation for the results of palladium exposed to a high-pressure deuterium gas in the hollow core of Arata-Zhang cathodes. The samples were from cathodes producing excess heat (10's of megajoules) over a several-month period of electrolysis [7]. A change in isotope ratio was definitely found but the conclusion was that a conventional explanation is hard to find.

In cold fusion research by electrolysis of Pd in heavy water, the experiments of Russian scientist Prof. Kanarev [25] and Japanese researcher Dr. T. Mizuno [14] provided measurable proof of fusion and fission products.

In Italy, the cold fusion research pioneered by Francesco Piantelli in 1989 [8] has been extended and supported by the local inter-university centers in Bologna (Focardi, Campari) and Sienna (Piantelli, Gabbani, Montalbano, Veronesi). A detailed report about this research was published by the Italian National Agency for New Technology, Energy and Environment in 2008 [9]. Piantelli filed two patents WO9520816 (1997) and

This monograph is a result of non-funded theoretical work

WO2010058288 (2010), describing different methods, and published an article ITSI920002 [8] about cold fusion of nickel with deuterium or hydrogen.

Recently, interest in cold fusion as an alternative to nuclear energy was raised by the successful demonstration of the Rossi cold fusion device called E-cat. The Focardi-Rossi method of nuclear reaction Ni + H -> Cu [10] is based on the preliminary research of Focardi and colleagues [11]. Sergio Focardi is an emeritus professor at the University of Bologna while Andrea Rossi is a skilled researcher and inventor. After years of successful collaboration, they gave on January 14, 2011, the first public demonstration of a nickel-hydrogen fusion reactor, called E-cat, capable of producing more than 10 kilowatts of heat power, while only consuming a fraction of that. In 2008 Rossi filed International patent application WO 2009/125444 A1 entitled Method and Apparatus for Carrying out Nickel and Hydrogen Exothermal Reaction [12]. Ignoring the skepticism in the main stream science, Rossi proceeded further with the development and manufacturing of his E-cat generator. Public demonstrations of the E-cat reactor with some invited experts were made on January 14, March 29, April 19 and 28, September 7, October 6 and October 28, 2011. During the larger public demonstration on October 28, 2011, Rossi invited a few dozen people, including a group of engineers from an unnamed potential US customer, as well as a handful of journalists. According to Rossi, each module received an initial energy input of 400 watts and produced a self-sustaining, continuous output of about 10 kilowatts per hour for the next few hours.

According to current understanding of nuclear physics, fusion may occur only at superhigh temperatures in the order of a million degrees, so there are three main objections against cold fusion: the lack of strong nuclear emissions, the mystery of how the Coulomb barrier is penetrated, and the lack of strong emissions of gamma or X-rays. These objections rely on the officially accepted theoretical understanding and, more particularly, on Quantum Mechanics which is based on the Bohr planetary model of hydrogen extrapolated to all atomic nuclei. According to this model, the nucleus is extremely small in the order of 10^{-15} m, so the Coulomb barrier at such a distance is extremely strong and can be overcome only with a very high collision momentum achievable at a temperature of a million degrees. Another argument against cold fusion is the lack of reliable proof of fusion by-products that always accompany the high temperature fusion or fission reactions. In the race to Cold Fusion, one of the first researchers to detect helium as a product of a nuclear reaction using palladium as a catalyst in a deuterium atmosphere was Dr. Les Case [13]. Other researchers repeated the experiment with different degrees of success, but a number of them claimed to have obtained helium. This means that a nuclear reaction D+D->He took place with other nuclear transmutations. This will be discussed in the next sections.

The conclusion is that unbiased scientific discussion in a search for a new theoretical explanation is highly necessary.

2. A new theoretical approach

2.1 Brief introduction

The feasibility of cold fusion was theoretically envisioned by Dr. Stoyan Sarg after he developed the BSM-Supergravitation unified theory (BSM-SG). After the first copyright protection in CIPO Canada in 2001 [15], the BSM-SG theory and related articles were posted in physical archives [16,17,18,19] and reported at a number of international scientific conferences. Scientific papers were published in Physics Essays [20], Journal of Theoretics [21] and conference proceedings [22,23]. The complete theory was published as a book in 2004 [24]. The BSM-SG theory is based on an alternative concept of the physical vacuum that has not been investigated before. The models developed as a result of the suggested concept are in excellent agreement with experimental results and observations in different fields of physics. The initial framework is based on two indestructible fundamental particles, FP, with parameters associated with the Planck scale and a fundamental Law of Supergravitation (SG). This law is distinguished from Newton's law of gravity in that the SG forces, F_{SG}, in pure empty space are inversely proportional to the cube of distance (while the gravitational forces in Newton's law are inversely proportional to the square of distance).

$$F_{SG} = G_0 \frac{m_{01} m_{02}}{r^3} \qquad \text{Supergravitation Law (SG)} \qquad (1)$$

where: G_0 – SG constant, m_{01} and m_{02} - SG masses (different than the Newtonian mass) , r - distance

The two FP particles combine in hierarchical formations of 3D structures held by SG forces. In far range propagation through the space-fabric of the physical vacuum, the SG forces become gravitational forces of

This monograph is a result of non-funded theoretical work

Newton's law of gravity. In contrast to the methods in Quantum Electrodynamics, the BSM-SG theory applies Classical Electrodynamics and the SG law. The suggested concept and derived physical models allow explanation of all kinds of quantum mechanical interactions between elementary particles, using a classical approach and the unveiled structure of both the particles and the space-time fabric. In this approach, the Heisenberg Uncertainty principle is not needed and so does not interfere with the logic of the analysis. The results reveal the missing relationships between Classical Electrodynamics, Quantum Mechanics, Special and General Relativity, and Cosmology.

The SG forces are not only behind the nuclear forces at a close distance between nucleons, but they also define the electrical field of charged particles. Since the elementary particles appear to have a 3D non-spherical structure and shape, the atomic nuclei also possess non-spherical 3D geometrical structures that define the row and column pattern of the Periodic Table. In this sense, one of the major results of the BSM-SG theory is a new vision of the 3D structure of protons and neutrons and their spatial arrangements in atomic nuclei. This is presented in the Atlas of Atomic Nuclear Structures (ANS) that was archived in the National Library of Canada [17] and published elsewhere (viXra:1107.0031).

2.2. Non-spherical shape of protons and neutrons and their spatial arrangement in atomic nuclei according to BSM-SG theory

In Quantum Mechanics (QM) and Particle Physics all particles are assumed to be spherical, so QM deals only with energy. This excludes the option that particles might have a denser non-spherical fine structure. The assumption of the spherical shape is based on the Bohr planetary model of hydrogen, despite that some of its enigmatic problems have not been solved from the time of its adoption. Based on scattering experiments in which only a spherical shape is assumed, the nucleus is considered extremely small in the order of 10^{-15} m. The main scattering experiments are two types: scattering of positrons from a positive atomic nucleus (or the proton in case of hydrogen), known as Bhabha scattering, or Rutherford scattering of alpha particles from a thin foil of gold. However, the scattering experiments have only angular, and not transverse, resolution. Then if the nucleus is assumed to be non-spherical, such as a torus, a twisted torus, or a folded torus with much larger toroidal radius but thinner, the scattering data by positrons will be one and the same. Also, the positrons as well as the electrons are found to have rotational speed, so the momentum of this will affect the interpretation of the scattering data. In the Rutherforth scattering experiment, if the Helium nucleus is not spherical, the data will be influenced by a channeling effect that also will contributing to a smaller angular dispersion. (This is illustrated by Fig. 8.22 of BSM-SG book).

If the shape of protons and neutrons forming the nuclei are not small spheres, then the strong nuclear forces will be spread over a much larger distance, but still inside a volume approximately equal to the volume of a sphere with a Bohr's radius $a_0 = 0.523$ Angstroms. For the real hydrogen nucleus, this volume may not have the shape of a sphere, but an ellipsoid, while in other atomic nuclei it might have a different shape. Then in the case of hydrogen, the QM energy levels will appear exactly the same as in the Bohr model, but the strong nuclear and Coulomb forces in that particular volume will have quite a different configuration. Such differences from the QM models will be valid for all atomic nuclei, since they are based on the Bohr planetary model. In this sense the QM models of the atoms appear to be not physical but mathematical. Then the real physical models of atomic nuclei could be completely different, and the Coulomb force at the center of the atomic nucleus will not converge to a small sphere with a radius of 10-15 m, but will have a much lesser strength spread in a non-spherical volume. This is exactly the case for the BSM-SG models of the stable elementary particles and atomic nuclei. Direct observations with the most powerful electron microscopes barely reach a resolution of 1 Angstroms (1x 10^{-10} m), which is still poor in comparison to the Bohr radius of hydrogen $a_0 = 0.523$ Angstroms. Despite this, some advanced electron microscope images begin to show features of a non-planetary atomic model (this will be discussed later). According to BSM-SG, the strong nuclear forces are from the SG forces defined by Eq. (1) for pure empty space. But in the space fabric of the physical vacuum (called a Cosmic Lattice in BSM-SG), for a distance smaller than the Bohr radius they may obtain a higher inverse power order of dependence on distance due to a leakage of the SG forces at closed proximity (discussed in Chapter 2, p. 2-17 of BSM-SG). The detectable signatures of the SG forces are the Casimir forces, some Van der Waal forces, and some observations in nanotechnology where single atoms put in a flat metal lattice stay in that place. Other observations are the clustering of the electrons in electron beams and the whole Quantum Hall effect at room temperature.

This monograph is a result of non-funded theoretical work

The success of Quantum Mechanics is undeniable and the QM models are convenient for calculation of energy interactions and optical spectra based on the energy levels, since the non-linearity of the nuclear forces is not apparent. However, a number of enigmatic problems are not explained by them. Additionally, the QM models cannot explain what defines the directions of the chemical bonds between molecules. If the QM models of atoms are not real, but mathematical, then we do not have to stick to the assumption that every elementary particle and nucleus has a spherical shape.

If the BSM-SG models of atomic nuclei are assumed as real physical models, for which there is a lot of proof in BSM-SG theory, then the QM models appear to be not real but mathematical models. In this sense, the BSM-SG atomic models provide a completely new approach for investigating the Coulomb barrier. The initial guess about the shape of the proton and neutron was intuitively obtained when analyzing the data from particle physics experiments. Why do the initially obtained unstable particles from the collisions of protons and neutrons, such as pions and kaons and their decay products to muons and electrons (positrons), exhibit so consistent masses? The logical answer is that these unstable particles might be enclosed inside of a torus, so when this torus is cut in just one place, the pions and kaons are also cut in one place. But in this new shape, they are unstable and undergo further decay. One big enigma not solved for many decades (due to the adopted concept of the physical vacuum) is that the sum of the masses of the first products (pions and kaons) is larger than the proton or neutron mass. The BSM-SG analysis discovered that the kaon structure, while still helical has a different overall shape from the helical structure of other particles (pions, muons, electron, positron), so it has a lower inertial mass property in the Cosmic Lattice space of the physical vacuum. This caused inaccuracy in the kaon mass estimation. Correcting this problem revealed the internal structure of the stable proton and neutron particles. The detailed analysis of Particle Physics data is presented in Chapter 6 of BSM-SG. Once the enigmatic problems about the shape and fine structure of the stable elementary particles (proton, neutron, electron and positron) were solved, everything from particle physics to cosmology became highly logical and understandable.

The question why the chemical and physical properties of the elements in the Periodic Table do not follow strictly the row and column pattern, has not been answered from the time of Mendeleyev. Could this be a signature of some three-dimensional composition of fractal structures from which the atomic nuclei are built? The extensive analysis of experimental data in different fields of physics led to revealing the shapes of the proton and neutron that perfectly match the arrangement of the elements in the Periodic Table. The proton has the shape of a twisted torus in the form of the figure 8, while the neutron is a double folded torus. Their shapes are different three-dimensional curves, but they have one and the same fine structure composed of helical structures (discussed in Chapter 6 of BSM-SG). In the BSM-SG theory, the validation of this conclusion involved extensive analysis of the Particle Physics data, and matching of the derived models with the theoretical developments of Quantum Mechanics, chemistry and experimental data from different fields of physics.

Figure 1 illustrates the revealed shape and the spatial arrangement of the protons and neutrons in the atomic nuclei of the elements Hydrogen, Deuteron and Helium according to the BSM-SG theory.

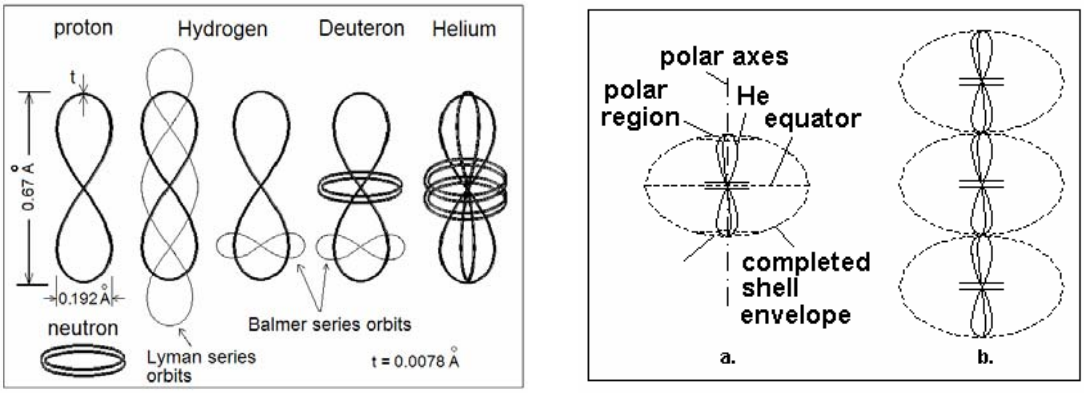

Fig. 1. Left side: shape of the proton and neutron and nuclear configuration of H, D and He atoms according to the BSM-SG theory, right side a.- completed shell of Argon (the envelope is shown), b. – a chain structure in heavier elements.

On the left side of Fig. 1, the atomic nuclei of the first few elements from the Periodic table are shown, while on the right side, the cluster chain structure of atomic nuclei with Z-number larger than 18 (Argon) is shown. When using the shape of the proton and neutron according to BSM-SG, and going through the Periodic

This monograph is a result of non-funded theoretical work

Table by consecutive increases of the z-number, we find an extraordinarily good match to the pattern of the Periodic Table of stable isotopes. In such an approach, the physical meanings behind the Hunds rule, the Pauli exclusion principle, the shell completion, valences, oxidation numbers, first ionization potential and X-ray properties are revealed for the first time. Additional new features of the nuclei are also revealed, putting a new light on the physics of the nuclear bonds, the completion of the shells and what defines the valences and the direction of the chemical bonds. These features are discussed in detail in Chapter 8 of BSM-SG. The revealed physical configurations of the atomic nuclei of all stable isotopes up to z = 103 (Lawrencium) are presented in the BSM-SG Appendix Atlas of Atomic Nuclear Structures (ANS), one of the major derivatives of BSM-SG, also published separately [17]. Figure 2 shows a graphical view of some selected atomic nuclei as derived in BSM-SG theory and included in the Atlas of Atomic Nuclear Structures [17]

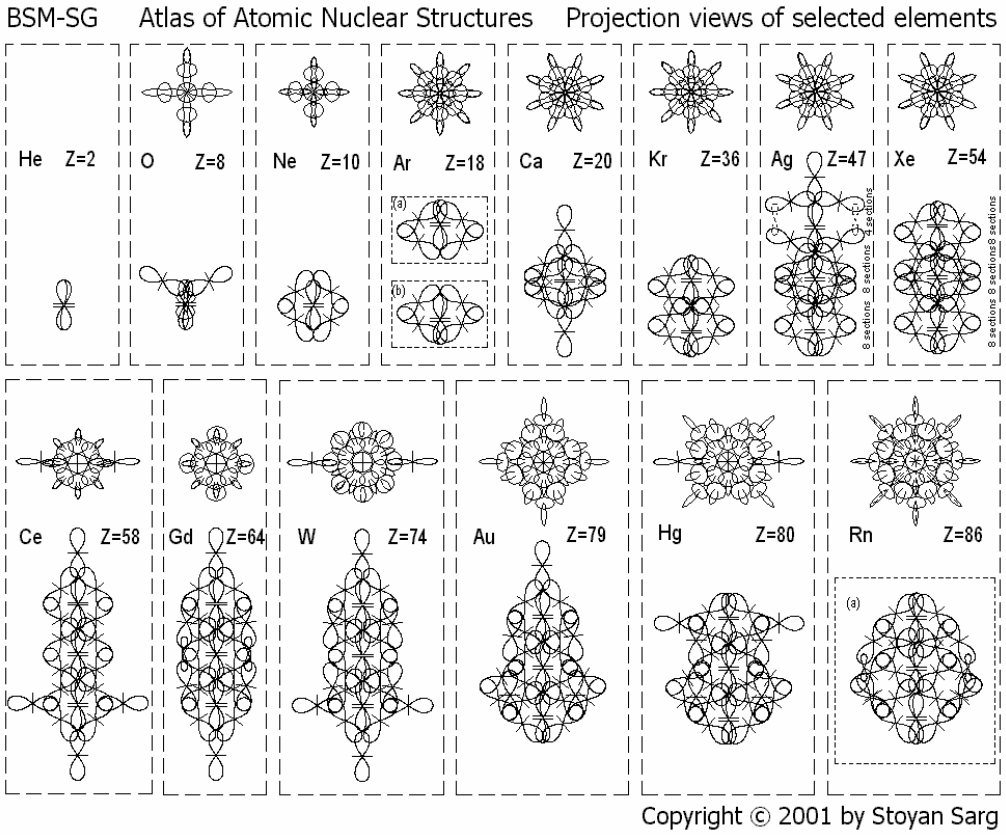

Fig. 2. Extract from the Atlas of the Nuclear Structures showing the graphical view of some selected atomic nuclei [17]

From Fig. 2 we see that the nuclear overall shape for elements with 18<Z<86 have not spherical but elongated shape. The protons (deuterons) in the completed shells have strong nuclear bonds GBclp and weaker EB bonds. (§8.3.6, Chapter 8 of BSM-SG). The element Ag has both types of bonds (see also Fig. 13). GBclp bonds are fully symmetrical along the polar axis providing a symmetrical Coulomb field, while the Coulomb field from EB bonds is more extended (see Fig. 13). The symmetrical arrangement of the Coulomb field plays an important role for the atomic arrangement in the metal lattice. They keep the orientation of neighboring atoms. The detectable signature of this orientation are the Laue patterns obtained by the X-rays spectroscopy. High resolution images from electron microscopy also confirm this.

The Russian professor Dr. Kanarev, a theorist and cold fusion researcher, also arrived at the idea that the atomic nuclei are not blobs of protons and neutrons but have a 3D spatial arrangement [25]. Some atomic nuclear models according to Dr. Kanarev [25, 26] are shown in Fig. 3. At first glance, there is a similarity between the BSM-SG models illustrated in Fig. 2 and the models of Dr. Kanarev shown in Fig. 3 in that the overall shapes of the atomic nuclei are not spherical. However, they are quite different. The protons and neutrons in Kanarev's models are interconnected spheres, while in Sarg's model they have a specific 3D geometry. There has not been any cooperation between Dr. Sarg and Dr. Kanarev and their theoretical approaches are quite different.

This monograph is a result of non-funded theoretical work

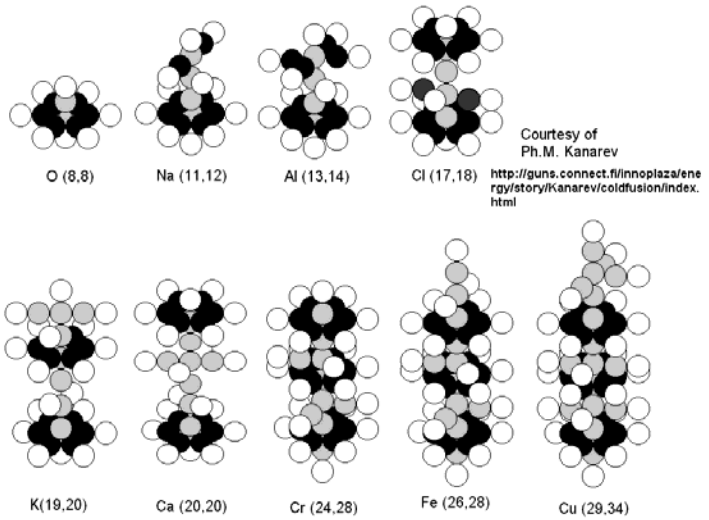

Fig. 3. Some atomic nuclei according to Dr. Kanarev. Courtesy of Kanarev [25,26]. The protons are shown by white spheres, the neutrons are shown by dark spheres in one sectional plane and grey spheres in a different sectional plane.

2.3 Coulomb barrier of the proton

According to BSM-SG theory, the SG forces are not only behind the nuclear forces. They also define the field lines of the electrical charge in closed proximity to the proton core. Therefore the SG field also defines the so-called Coulomb barrier that is one of the most controversial issues in nuclear fusion. Fig. 4 illustrates the distribution of the electrical field (E-field) in close proximity to the proton's high-density core and the locked E-field around the neutron's high-density core.

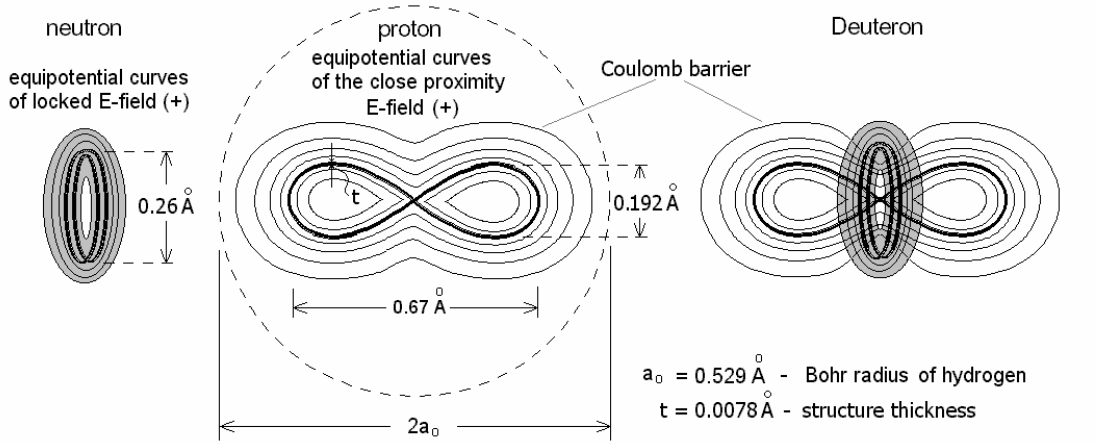

Fig. 4. Graphics illustration of the Coulomb barriers of the proximity E-field of the proton and the locked E-field of neutron. Both, the proton and neutron create the E-field as a modulation of the physical vacuum (CL space) by the superfine dense helical structure of their cores. The E-field of the neutron, however, is locked in proximity due to the anti-symmetry of the modulation field from the double folded torus core. This could be easily visualized if using the torus of a wound spring.

The electrical charge in closed proximity to the proton is distributed around its shape, but this is in a microscopic range smaller than the Bohr radius and its shape could not be detected by existing technology. Outside of the Bohr radius, the E-field lines appear as coming from a point charge. In fact the electrical charge is caused by modulation of the physical vacuum by the strong SG forces of the superdense helical structures of the proton's core. The neutron, despite having the same superdense core, does not exhibit a detectable electrical charge because its shape of a double folded torus makes the modulation of the physical vacuum anti-symmetric, so the electrical charge is closed in proximity. The signature of this locked charge appears only when the neutron is in motion, when it also exhibits a magnetic moment that is an enigma in Modern Physics. The spatial configuration of the proton's Coulomb barrier illustrated in Fig. 4 is significantly different from the Coulomb barrier of the Bohr model of hydrogen. Furthermore it could be modified to some extent due to its dependence on the SG forces, and there are some technical methods for causing such an effect.

This monograph is a result of non-funded theoretical work

In fact, the core internal structure of the proton and neutron has the features of a spring. It is well known that a single neutron is not stable and converts to a proton with a lifetime of 12 min. The instability is caused by the weak balance between the repulsive E-field forces in the locked E-field and the attractive SG forces that keep its shape of a double folded torus. However, when the neutron is over the proton saddle (central section) it is stable, forming in such way the stable element Deuteron. The stability is a result of a stronger balance between the repulsive E-fields (+) of the proton and the locked, but accessible at such a distance, E-field (+) of the neutron. This is graphically illustrated on the right side of Fig. 4. The neutron can only rotate or vibrate, and the latter is behind a physical phenomenon known as the Giant resonance. This phenomenon, discovered by Baldwin and Klaiber in 1947, was later confirmed by many and interpreted by Goldhaber and Teller (Phys. Rev. 74 (1948) 1046). It was based on the assumption that the protons in the nucleus move in one direction while the neutrons move in the opposite direction. When two neutrons are over the saddle point of a proton, the obtained nuclear structure is Tritium. The bonding energy of this three-body system is not as strong as for Deuteron, because the two neutrons are separated by a gap due to their locked repulsive E-field (+) so they are away from the E-field valley of the proton. The separation distance calculated in §6.14.1, Chapter 6 of BSM-SG is 0.107 Angstrom which is about 16% of the proton length (0.667 Angstrom). When the Tritium nucleus is included in the heavier atomic nuclei, however, it is stable because the other protons' E-fields modify the Coulomb field of the host proton.

In accordance with the BSM-SG model, the process known as electron capture ($p + e^- \rightarrow n$) is just a folding of the twisted shape of the proton until it obtains the shape of the neutron as a double twisted torus, held in this shape by the SG forces. Then the charge in the far field disappears. This happens in some nuclear reactions and especially in the radioactive decay of the fission chain reactions leading to unstable nuclei. One of the first of such processes experimentally invoked is the Don Borglhi experiment known as a "synthesis of neutrons from protons and electrons" at low energy. The BSM-SG model also provides an answer to the long standing problem of the "missing neutrino" from the Sun. The resulting locked E-field of the neutron in the conversion of the proton to a neutron is wrongly attributed to the emission of a neutrino particle.

From the graphical model of the Coulomb barriers in Fig. 4 it is evident that a nuclear reaction $p + d \rightarrow D$ would take place if the neutron and protons are properly oriented and the proton's Coulomb barrier is slightly modified. Technical methods for this possibility will be discussed.

2.4. Evidence for some features of the BSM-SG atomic models from some high-resolution electron microscope images

The E-field lines outside of the sphere defined by the Bohr radius (for hydrogen) will appear as coming from a point charge. Electron microscopes, for theoretical and practical reasons, cannot sense the region inside of this sphere. However they may detect some non-uniformity of a single sheet lattice that is not explainable by Quantum Mechanical models of atoms. Such examples are electron microscope images of the lattice structure of a carbon nanotube [27] (Fig. 5.a.) and a graphene [28] (Fig. 5.b). Panel b. in Fig. 5 shows the original image of graphene, while Panel c. shows the same image processed to fit the display brightness scale. Fig. 5.d shows the sketch of the carbon nucleus according to BSM-SG. The protons p_3 and p_4 are in the drawing plane, while the protons p_1 and p_2 (shown smaller) are in a perpendicular plane.

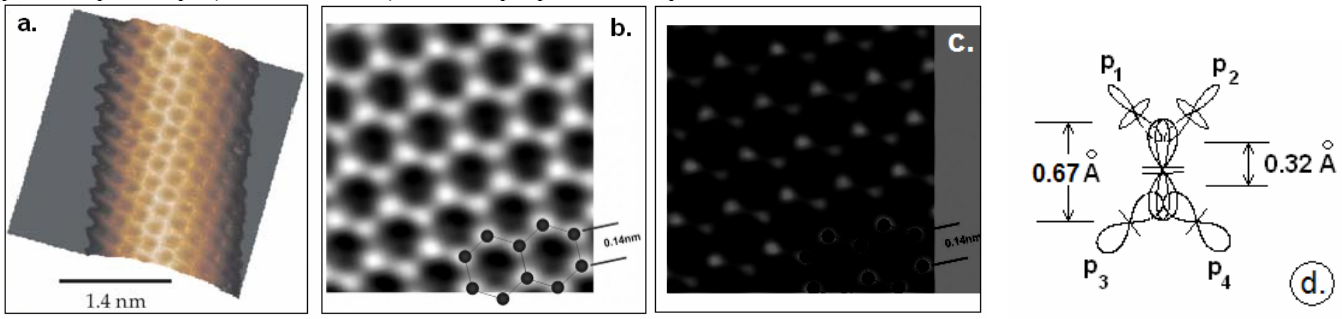

Fig. 5 a. Single-wall nanotube (Courtesy of A. Javey et al.) [,27],
b. Single wall Carbon sheet with TEAM microscope [28]
c. Processed image by brightness adjustment,
d. Sketch of the carbon nucleus (p3 and p4 lie on a drawing plane, p1,p2 are perpendicular to the drawing plane

This monograph is a result of non-funded theoretical work

According to QM models the connecting bonds of carbon should lie in one plane, but according to the BSM-SG model, they do not. This means that a single sheet of carbon atoms will show displacement of every neighboring atom. If building a 3D model using the 3D model of carbon, shown in Fig. 5.c, we would find that they lie in two parallel planes separated by a distance smaller than 0.5 Angstroms. Panel a. shows a lattice that is not smooth, while Panel b. shows a lattice plane displacement.

2.5. Radioactive alpha decay in the heavier elements as a cold fusion between deuterons

Since the protons in the atomic nuclei are in a closer range than the space defined by the proximity E-field of the free proton shown in Fig. 4, their Coulomb barrier is distorted. This means that in the heavier atoms a spontaneous fusion between deuterons might take place with some probability. This happens naturally in the large atomic nuclei with Z > 57 (beginning from the Lanthanides) and the process is known as a radioactive alpha decay. Based on the 3D nuclear configuration, Stoyan Sarg showed theoretically in 2002 that the alpha decay in the heavier elements is preceded by a process of fusion of protons and neutrons into a helium nucleus [18]. Fig. 4 shows the position of the two deuterons in the atomic nucleus of Gadolinium (Gd).

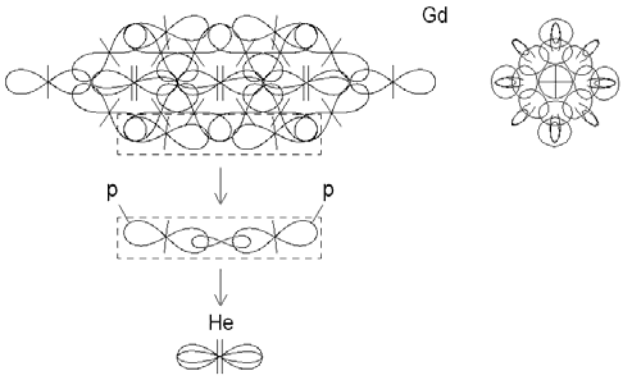

Fig. 6. Alpha decay of Gd. The position of the two deuterons are shown prior to their fusion into helium nucleus.

The two deuterons fuse into a He nucleus – an alpha particle at room temperature. Consequently, cold fusion at room temperature is possible under special conditions.

2.6. How the valence protons (deuterons) of the atomic nuclei define the chemical bond directions in the molecules in agreement with the VSEPR models in structural chemistry.

The BSM-SG atomic models also have other important features. The nucleus of every element has a well-defined rotational symmetry around an axis that we may call a polar axis. Another feature is that every atomic nucleus with a Z-number larger than one has at least one helium nucleus in the middle of its nuclear structure because helium has the densest atomic nucleus. The heavier atomic nuclei have more than one He nucleus and they are aligned with the polar axis as a chain (see Fig. 1 b.). Most of the protons and neutrons are combined in deuteron nuclei but some single protons also exist in the nuclei. In atomic nuclei with z > 2 and especially the heavier elements, tritium nuclei are also included but the embedded tritium is stable. The internal nuclear shells are tightly bound and do not participate in chemical reactions, but the deuterons or protons from the external shells provide the chemical valences. One important feature of the valence protons (deuterons) from the external shell is that one end is bound to the polar spot by SG forces, while the other end has a limited angular freedom in a plane passing through the polar axis. However, they have a tight angular restriction in any perpendicular plane. The angular freedom is largest in Oxygen, so it defines the chemical feature known as oxidation strength. Analysis of some simple molecules using the BSM-SG models is presented in Chapter 9 of BSM-SG. The angular positions of the valence protons (deuterons), combined with the 3D geometrical shape of the nuclei, define the angular positions of the chemical bonds. Another important feature of revealed atomic structures is that the electrons do not form arbitrary clouds. They move in individual quantum electron orbits whose positions and traces are defined by the close proximity electrical field of the proton, so they are bound to the protons (deuterons). The quantum orbits are in a strong SG field with a non-linear gradient, so the orbits for the different energy levels are quite close. Since valence protons (deuterons) have an angular freedom in a plane passing through the polar axis, protons from the opposite poles of a single chain element sharing one and the same restricted meridian section become connected by one quantum orbit, so they are excluded from the principle

This monograph is a result of non-funded theoretical work

valence. All these features of the atomic nuclei are clearly evident from the atlas ANS, if following the trend of Z-number increase.

2.7. Why the nuclear chain reactions induced by neutrons leads to so many radioactive byproducts.

It is well known that for the stable isotopes the increase in the number of neutrons is faster than the Z-number (protons) increase. This enigma is not explainable by QM models of atomic nuclei. BSM-SG models provide an explanation based on the discovered problem referenced as a "polar region problem" (§8.3.7, Chapter 8 of BSM-SG). It is caused by the closer accumulation of proximity E-fields from the protons at the polar region when the Z-number increases. According to BSM-SG this is naturally compensated by accumulation of more neutrons in the equatorial region. This modifies the E-fields in the polar regions (due to SG forces) making the isotopes more stable. The excess neutrons are bound in deuterons and tritium nuclei. However this trend must match the rotational symmetry of atomic nuclei. It has some relation to the nuclear spin number and it is important for stability. As a result some elements have more stable isotopes, while others do not. Technetium, for example, is an element that does not have a stable isotope. Examining the Z-trend increase in the Atlas of ANS we may see that the spatial arrangement of the protons (deuteron, tritium) has a quite good rotational symmetry.

It is well known that the nuclear chain reaction requires not fast but slow neutrons. Why is this? It is also known that the slow neutrons are embedded for a short time in the recipient nuclei. They make them unstable and they decay to other unstable nuclei. Having in mind that the positions of the neutrons in the stable isotopes are highly symmetrical in respect to the polar axis, there is a very low probability that the captured neutron will be in the right place. That's why the nuclear chain reaction provides a lot of radioactive byproducts with different decay times, but most being very short. This is in sharp contrast to cold fusion where radioactive byproducts are very rare or absent. All presently existing nuclear power plants are based on nuclear fission chain reactions that are responsible for accumulation of a large amount of radioactive waste.

2.8. Unit charge. Structure of the electron and trace lengths of the quantum orbits

Quantum Mechanics cannot provide answer about the enigma: why do the proton, electron and other elementary particles with different masses have one and the same unit electrical charge? Such explanation is suggested in BSM-SG §2.15.2, Chapter 2 of BSM-SG. The charge is not a substance contained inside of the particle, but a kind of modulation of the CL space (physical vacuum). Since all elementary particles are comprised of two types of helical structures in which the SG field is involved, an accurate balance is always maintained so particles with different masses appear to have one and the same unit charge. These two types of helical structures could be additionally twisted, but they are stable if they are connected in a loop that might also be twisted or curled (see Chapter 6 of BSM-SG for more details).

The Quantum orbits in the BSM-SG models of atoms are derived by the unveiled material structure of the electron presented in Chapter 3 of BSM-SG and published in the peer review Journal Physics Essays [20]. The overall shape of the electron has some similarity to the shape suggested by the Nobel laureate Arthur Compton as a torus with a Compton's radius, but at the same time it is quite distinguished. The revealed shape of the electron is a cut torus having a small helical step, while it also possesses a fine structure made of helical structures. The external helical structure modulates the CL space (physical vacuum) by creating a negative electrical charge. The electron and its fine helical structure according to BSM-SG is graphically illustrated in Fig. 7, where R_c - is the Compton's radius, s_e – is the helical step of cut torus.

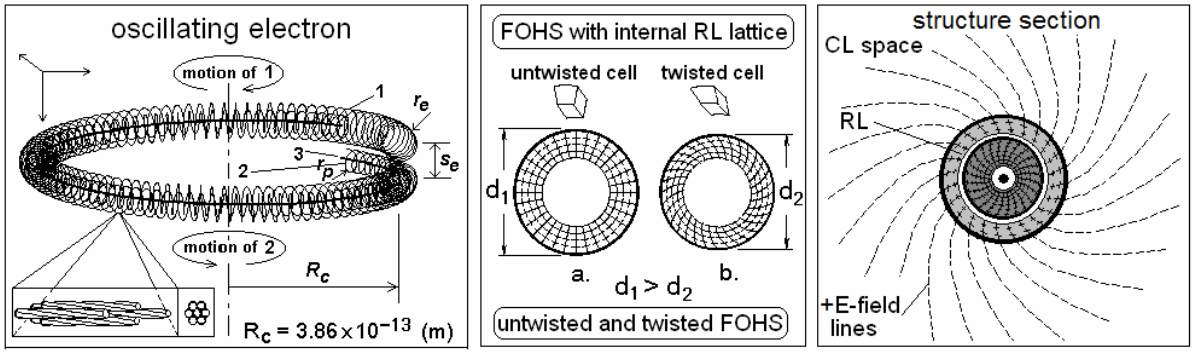

Fig. 7. Structure of the electron according to BSM-SG

This monograph is a result of non-funded theoretical work

The electron is a 3-body system, exhibiting rich oscillation properties. When interacting with the CL structure of the physical vacuum, this physical model exhibits all known QM properties of the electron. Let us suppose that the structure of the electron moves as a screw, so that the peripheral velocity is equal to the speed of light and it makes one revolution for a Compton time. Then the axial velocity is

$$\upsilon = \frac{cs_e}{\sqrt{4\pi^2 R^2 + s_e{}^2}} \tag{2}$$

This screw type of motion obviously is optional and let us suppose that it corresponds to the electron motion in Bohr atom at orbit a_0 with energy of 13.6 eV. Then the axial velocity is

$$\upsilon = \frac{e^2}{2h\varepsilon_0} = \alpha c = 2.18769 \times 10^6 \quad (m/s) \tag{3}$$

where: e – charge of electron, h – Planck constant, c –speed of light, α - fine structure constant

Solving (2) and (3) and substituting $2\pi R_c = \lambda_C = c/\nu_C$ we obtain

$$s_e = \frac{\alpha c}{\nu_c \sqrt{1-\alpha^2}} = \frac{c\lambda_c}{\sqrt{1-\alpha^2}} \qquad s_e = 1.77 \times 10^{-14}\ (m) \qquad \text{helical step} \tag{4}$$

where: $\nu_c = 1.2356 \times 10^{20}$ (Hz) - Compton frequency, λ_c - Compton wavelength

It is known that the electron possesses a magnetic moment anomaly whose theoretical value is $0.5\alpha/\pi$, but its physical explanation has been an enigma so far. According to Eq. (4) this is the helical step, so the fine structure constant appears embedded in the structure of the electron.

The dimensionsless fine structure constant appears in many interactions in Quantum Mechanics and Particle Physics. According to BSM-SG model it is a ratio of two cycles of spatially vibrational modes of a tetrahedron from the spherical FPs in the Planck scale range, so it is at the lowest level of matter organization. At this micro-scale range, only the SG forces are present. This is discussed in (§12.A.5.3 Chapter 12 of BSM-SG), where a theoretical equation (5) for the fine structure constant is derived providing a quite accurate value in comparison to CODATA 98 value for n = 137. Such tetrahedra are embedded in the fine structure of all elementary particles including the space-time fabric. For this reason, the fine structure constant appears in many interactions.

$$\alpha = 2/[(n^2 + 2\pi^2)^{1/2} + n] = 7.29735194 \times 10^{-3} \tag{5}$$

$$\alpha = 7.297352533 \times 10^{-3} \qquad \text{according to CODATA 98} \tag{6}$$

At the same time when the electron performs a screw-like motion with axial velocity αc corresponding to 13.6 eV, the structure of electron oscillates with its first proper frequency equal to the Compton frequency. This is an optimal quantum velocity in which the phase of the oscillating electron matches the phase of the SPM vector (Spatial Precession Momentum) – a characteristic feature of the Cosmic Lattice node, which spatially oscillates with a Compton frequency (§2.9, Chapter 2 of BSM-SG). The phase propagation of the SPM vector in CL space (physical vacuum) is behind the constancy of the constant speed of light. The next lower quantum velocity is $\alpha c/2$ corresponding to electron energy of 3.4 eV in which the phase of the oscillating electron matches the SPM phase at every second turn of the rotating electron. The next lower velocity is $\alpha c/3$ corresponding to 1.51 eV with a phase matching at every third turn and so on. This screw-type oscillating motion of the electron, referred to as confined motion, defines preferred quantum velocities, which appear as energy levels in the hydrogen atom. Consequently, the principal quantum numbers of the Bohr model of hydrogen are in fact signatures of the motional behavior of the electron structure in the fabrics of the physical vacuum.

From the confined motion of the electron, a Quantum Efficiency factor is directly derivable as $\eta = (1 - v^2/c^2)^{1/2}$ (§3.11.A.1, Chapter 3 of BSM-SG). Its inverse value is the relativistic gamma factor. For velocities larger than αc the electron rotation is slower, so the tangential velocity never exceeds the speed of light. Then the inverse factor η becomes the relativistic gamma factor. The quantum interactions with the CL space make the motion with higher velocities more difficult, which explains the relativistic mass increase predicted by Einstein.

This monograph is a result of non-funded theoretical work

When the electron moves in a closed trajectory, the phase match between the SPM frequency of the CL structure (physical vacuum) and the two proper frequencies of the electron defines two important parameters of the quantum orbit: its trace length and the duration (a lifetime of the excited state) [20]. Therefore, the quantum orbits have different trace lengths for different quantum velocities of the electron. They are valid also for the chemical bonds in molecules that exhibit vibrational-rotational spectra, so they are illustrated in Fig. 10 together with some simple molecules.

In §7.8.2 Chapter 7 of BSM-SG, the Balmer model series of hydrogen is derived based on the BSM-SG model in which the strong SG field is involved. The calculated energy levels match the energy levels of the Bohr model of hydrogen. In fact the SG field defined by Eq (1) is for pure empty space. In physical vacuum (not empty space), when the distance between the proton and electron is quite close, the SG forces become inversely proportional to distance in order higher than 3 (due to the SG field leaking between the nodes of the CL structure). This, however, is consistent with some Van der Waal forces and Casimir forces experiments. Another important feature is that the electron orbits in the BSM-SG model of hydrogen are much more closely packed in comparison to the Bohr model. This is because, according to Newton's second law, the radius of the electron motion in a circular trajectory (in Bohr model) is inversely proportional to the square of velocity, while in the BSM-SG model it is inversely proportional to the velocity (due to the SG field). However, the length of the quantum orbit for 13.6 eV in the BSM-SG model is equal to the length of the Bohr orbit defined by the Bohr radius $a_0 = 0.52918$ Angstroms. The shape of the orbit, however, is not circular but follows the equipotential curve of the close proximity E-field of the proton. This explains the p-shapes of the wave functions observed in hydrogen, a feature that cannot not be explained by the Bohr planetary model using the classical electrodynamics. Two distinctive positions of the quantum orbits in hydrogen corresponding to the Lyman and Balmer series are shown in Fig. 1.

During the finite lifetime of the electron in a particular quantum orbit, it modulates the CL space by dissipating energy and, when dropping to a lower quantum orbit (lower energy level), the dissipated energy is released as a photon. This explains what is behind the Heisenberg Uncertainty Principle in Quantum Mechanics – the photon energy is not emitted directly from the electron, but from the space fabric containing the pumped energy from many orbital cycles.

In the internal shell of the heavier atoms, the strong SG field also contributes to the energy levels. The signature of this is the smooth increase of the Lamb shift with the z-number (number of protons) of the elements. If plotted against the atomic mass, the Lamb shift is not so smooth. This indicates that the electrons in the atomic nuclei are circling around the proximity field of the protons.

Fig. 8 a. and b. show two states of the hydrogen molecule H_2. In the state shown in a. and referred to as an ortho-state, the two protons are connected by a single quantum orbit with two electrons counter-circling in the orbit. The vibrational levels for this state are shown in Fig. 8 c. They are calculated by Eq. (7), which is a pure theoretical derivation, presented in §9.7, Chapter 9 of BSM-SG. They are compared and plotted together with the two energy levels (corresponding to two orbital spins) and estimated from the corresponding energy levels identified by the photoelectron and optical spectra. In the other state of H_2 shown in b. the two protons are connected by two separate orbits.

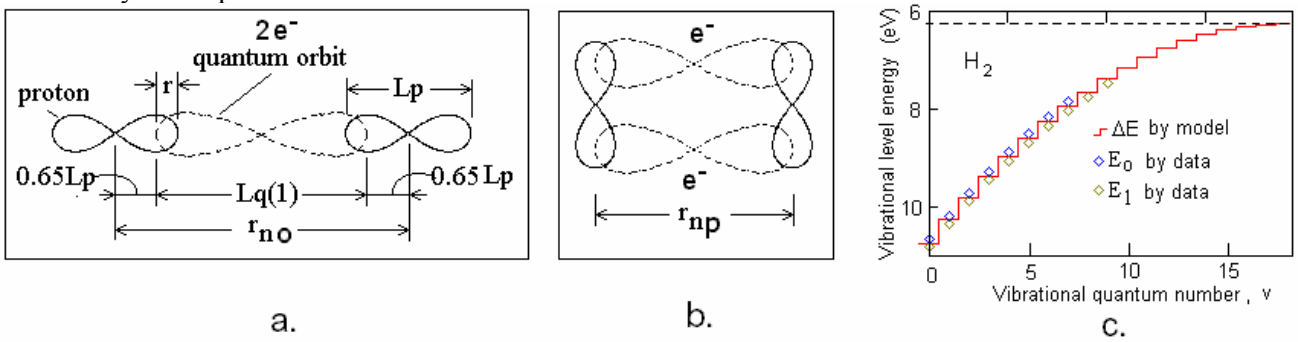

Fig. 8. a. – shape of H_2 molecule ortho-state, b. shape of H_2 molecule para-state, c.- energy levels by the BSM-SG model for ortho-state H_2 molecule and its match to experimental data

The parameters of the ortho-state H_2 molecule (shown in Fig. 5.a) were obtained in §9.6 of BSM-SG by analysis of the photoelectron [29] and optical [30] spectra. Using the total energy balance in which SG field energy is included, the expression (7) is derived (§9.7 of BSM-SG) providing the vibrational energy levels. This

This monograph is a result of non-funded theoretical work

expression involves the total SG energy balance that includes the SG attraction, the kinetic energy of the electron E_k, the energy of the proton charge E_q, and the molecular binding energy. The vibrational energy E_V is plotted in Fig. 8.c together with the energy levels corresponding to the identified corresponding optical spectrum band of the H_2 molecule. The calculated energy levels are in excellent agreement with the experimental data.

$$E_V = \frac{C_{SG}}{e[[L_q(1)(1-\alpha^4\pi\Delta^2)]+0.6455L_p]^2} - \frac{2E_q}{e} - \frac{2E_k}{e} + E_B \qquad (eV) \tag{7}$$

$$C_{SG} = G_0 m_0{}^2 = (2h\nu_c + h\nu_c\alpha^2)(L_q(1)+06455L_p)^2 = 5.2651\times10^{-33} \tag{8}$$

where: e – unit charge, $L_q(1) = 2\pi a_0 = 3.325\ \overset{0}{\text{A}}$ – quantum orbit length for electron velocity of 13.6 eV, $L_p = 0.667\ \overset{0}{\text{A}}$ – proton length, E_q = 511 KeV – unite charge energy, E_k – electron kinetic energy, v_c – Compton frequency, α - fine structure constant, G_{SG} – SG constant, m_0 – SG mass of the proton (also neutron), $E_B = 6.26\ eV$ - energy difference between the dissociated limit and the metastable state, $\Delta = (V_L - x)$ - vibration level (V_L – plotting vector origin, x – argument)

The state of the H_2 molecule shown in Fig. 8.b is called a para-state in BSM-SG because the protons' axes are parallel. They are connected by two quantum orbits with a single electron in each one. The internuclear distance is slightly smaller in comparison to the ortho-state until the SG attractive forces become equal to the Coulomb repulsive forces (both fields are distributed around the proton's shape and get higher order of dependence on distance. The energy balance for the ortho-state requires a more complicated method that is not a subject for this article. The shape of quantum orbits is slightly modified but they have the same trace length defined by the electron motion with energy of 13.6 eV (this is included in the system energy, it is not an energy level according to QM models). The para-state of the H_2 molecule is more compact so it is more stable against collisions from Brownian motion. So in a normal H_2 gas, the para-state dominates. The ortho-state according to BSM-SG corresponds to the "magnecular" gas suggested by R. Santilli [31].

The analysis of H_2 and D_2 molecules permitted the derivation of one important physical parameter of the SG law denoted as C_{SG} (Eq. 8). It is a product of the SG constant G_0 and the square of SG masses m_0 of the two protons. The ratio between C_{SG} and the similar product of the gravitational constant and the square of the proton mass, shows that the SG forces at nuclear distance are enormously strong.

$$C_{SG} \big/ G m_p{}^2 = 2.82\times10^{31} \tag{9}$$

The obtained value of C_{SG} is additionally verified in §6.14.1, Chapter 6 of BSM-SG, where it was used for theoretical calculation of the binding energy of the proton and neutron in the Deuteron. The estimate is based on a classical approach similar to calculation of the Newtonian gravitational potential but using the SG law instead. The applied approximate method is illustrated in Fig. 9.

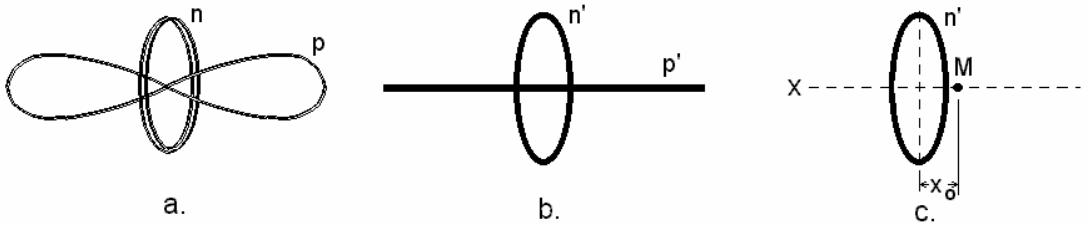

Fig. 9. a. The nucleus of Deuteron, **b.** – an equivalent model where the neutron SG mass is presented as a mass ring and the proton SG mass as a mass bar., **c.** – additional simplification by presenting the SG mass bar as a SG mass point.

The binding energy is equal to the disintegration energy when separating the proton and neutron along the axis of symmetry *x*, while using the SG law defined by Eq. (1). Since the SG force falls quite fast with distance, the estimation gives an accurate enough value for a separation at a distance equal to the size of the proton of 0.667 Angstroms. A theoretical estimation of the binding energy between the proton and neutron in the Deuteron was provided for the first time in §6.14.1. of BSM-SG. The estimated value is $2.145\text{x}10^6$ (eV) and it is quite close to the experimentally measured value $2.22457\text{x}10^6$ (eV). A similar approach was used in §6.14.12, Chapter 6 of BSM-SG for estimation of the separation distance between the two neutrons over a proton, which is a Tritium. The obtain value is 0.107 Angstrom which is about 16% of the proton length (0.667 Angstrom).

This monograph is a result of non-funded theoretical work

The analysis of the molecules in Chapter 9 of BSM-SG indicates that the derived structure of a simple H_2 ortho molecule participates as a chemical bond system in the molecules that have vibrational rotational spectra. A similar expression as Eq. (7) was derived also for the D_2 molecule, which is a more common system in the chemical bonds. The single deuteron is shown in Fig. 1. The ortho-state of the D_2 molecule has the same internuclear distance as the H_2 ortho-state shown in Fig. 8. For the D_2 molecule, the accurate fit of calculated energy levels to the optical vibrational levels appears when the product $\alpha^4\pi\Delta^2$ is divided by a factor of 2, which is a signature of the ratio between the nuclear spin of the deuteron and hydrogen. Then a universal expression (10) for internuclear distance, r_n, is derived for simple diatomic molecules. From the analysis in §9.75.D (Chapter 9 pf BSM-SG) it becomes apparent that the real vibrational range is negligible in comparison to the internuclear distance r_n, due to the inverse cubic SG forces involved.

$$r_n = (A - p)[(2\alpha C_{SG})/(pB_{D2}(n))]^{1/2} \qquad (10)$$

where: A – a nuclear mass expressed by the atomic mass unit (per one atom), p – number of protons involved in the chemical bond (per one atom), n – subharmonic quantum number of the orbit, B_{D2} – energy of D_2 bonding system; α - fine structure constant

2.9. Example of simple molecules illustrating the chemical bond direction and restricted freedom of the valence protons (deuterons).

Fig. 10. shows BSM-SG atomic models for simple molecules (obtained by analysis of photoelectron and optical spectra) with internuclear distance calculated by Eq. (10) that matches the proper size from the available sets of quantum orbits.

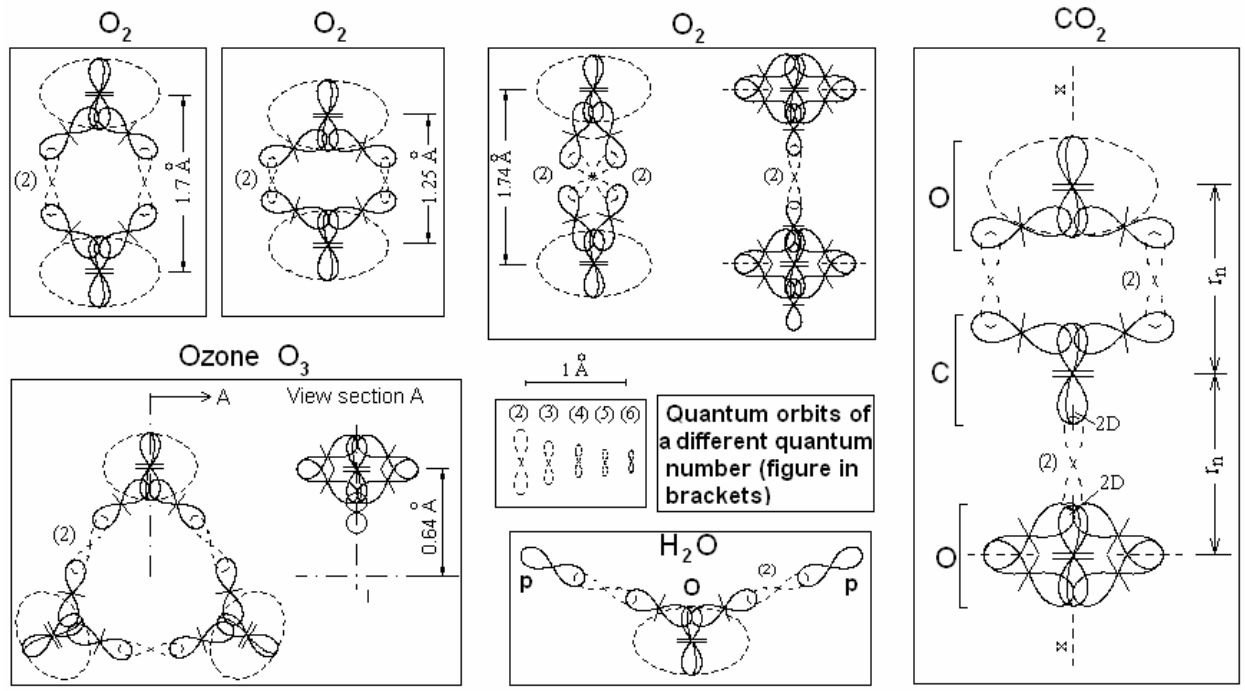

Fig. 10. Simple molecules: O_2 (3 different states), O_3, H_2O and CO_2 shown by the BSM-SG atomic models. For CO_2 molecule the viewing symmetry in respect to the horizontal axis gets a mirror change if the molecule is rotated around the vertical axis at 90 degrees. The neutrons are shown by a straight lines crossing the protons.

In the calculation of internuclear distance by Eq. (8), the possible quantum orbits have to be taken into account, while verifying the results with the optical and photoelectron spectra. The distance estimated in that way is in good agreement with the experimental value of the bond lengths (accepted in QM models).

We see that the angular positions of the deuterons in the two states of the oxygen molecule shown in the upper left side of Fig. 10 are slightly different (detailed analysis in §9.16, Chapter 9 of BSM-SG). The limited angular freedom of the valence protons (deuterons), combined with considerations of the quantum orbit lengths,

This monograph is a result of non-funded theoretical work

defines the angular positions of the chemical bonds and is in full agreements with the VSEPR model used in structural chemistry.

2.10. General Relativity (GR) from the point of view of BSM-SG theory and a hypothesis of GR field micro-curvature around atomic nuclei.

According to General Relativity (GR), a massive object creates a field curvature (the space is shrunk). The radial dependence of this shrinkage is asymptotically smooth. Let us consider two spherical zones with finite thickness centered on the massive object and denote them as near and far zones. The photon emitter or the observed event could be in the near zone and the observer in the far zone or vice versa. Now we need to find an etalon for unit distance. It must be some characteristic parameter available in both zones. In the optimal confined motion of the electron with energy of 13.6 eV for one full turn, its cycle matches the phase of the external SPM cycle and the trace length of the curve is equal to the Compton wavelength $\lambda_C = 2\pi R_C$. So the Compton wavelength is equal to the SPM wavelength and this equivalence should be valid for both the near and far zones of the space curvature (the electron Compton cycle is adjustable). Since the Compton wavelength is directly related to the Plank constant h by the expression $E = hc/\lambda$, it could be considered as a unit length etalon for measuring the energy of the emitted photon that passes between the two zones.

In the near zone the Compton wavelength etalon will be shorter than in the far zone. Then the wavelength of the photon emitted in the near zone but detected in the far zone will be gradually expanded, so it will exhibit a red shift. The wavelength expansion will be valid for the entire EM spectrum range since the photon wavelength is a whole number of Compton wavelengths. This explains the gravitational red shift of the photons generated near the Sun and observed at the Earth. From this explanation we may formulate one important conclusion:

(A). The field curvature of space (physical vacuum) possesses the property of conserving energy.

We will discuss this conclusion further in section 2.11. If the GR effect of field curvature does not have a limit, we may assume that such an effect may exist also in the microscale range due to accumulation of the superdense structures of the elementary particles in the atomic nuclei. In fact, a detectable signature of field curvature in close proximity to atomic nuclei exists. This is the experimentally measured Lamb shift corresponding to the transition $2S_{1/2} - 2P_{1/2}$. It is in contradiction to the Dirac definition that these two energy levels must be the same, and in QED it is often attributed to the finite size of the atomic nuclei and vacuum polarization. The Lamb shift, first discovered for hydrogen by Lamb and Rutherford in 1947, was investigated and measured for elements with Z>2, which are ions with only one electron. According to the Coulomb law, if the single electron is in such a strong field, the potential should increase linearly with Z-number. The observations, however, show that the Lamb shift increases with Z-number somewhat steeper than Z^3. Fig. 11 shows the Lamb shift in μeV for the elements from hydrogen to zinc. The data are from the article by Glen W. Erickson [32] recommended by NIST.

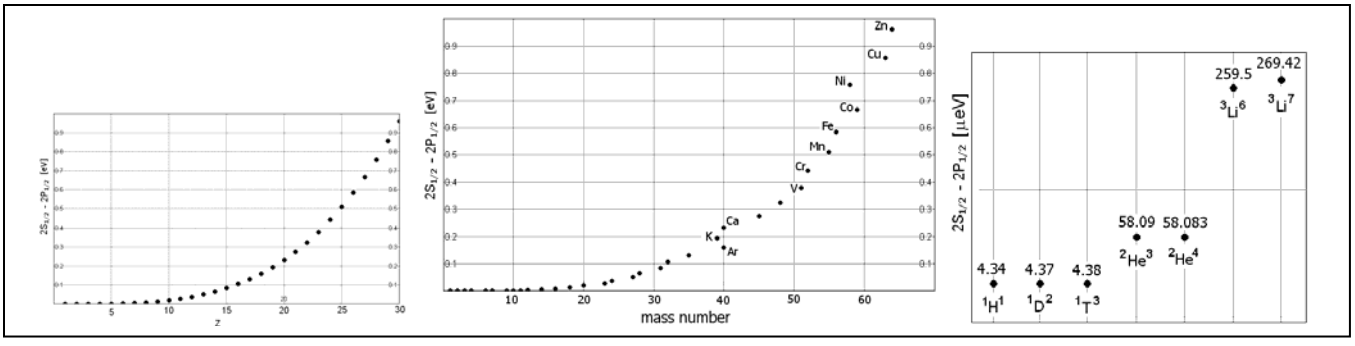

a. b. c.

Fig. 11. a.- Lamb shift as a function of Z-number, b. - Lamb shift as a function of mass number, c. – Lamb shift for the first few elements

Fig. 11. shows that the Lamb shift dependence on Z – number is smooth, but its dependence on the mass number (protons + neutrons) shown in Fig. 11. b. is not smooth. In the latter case, there is also an anomaly, as shown for K, Ar and Ca. This anomaly is consistent with the change in the K-edge level

This monograph is a result of non-funded theoretical work

of the X-ray mass attenuation coefficient discussed in §8.4.1, Chapter 8 of BSM-SG. In fig 11.c we see that the changes in Lamb shift from $^1H^1$ to $^1D^2$ to $^1T^3$ are insignificant, but the change at $^2He^3$, where the two protons fuse into a He nucleus (see Fig 1) is significant. Then the Lamb shift slightly decreases at $^2He^4$ from the added second neutron over the two protons. The jump of Lamb shift at $^3Li^6$ indicates the addition of a new proton at the polar region. Then it slightly increases after a neutron is added over that proton in $^3Li^7$. For higher Z-numbers, the accumulation of neutrons also contributes to the increase in the Lamb shift but less than the protons. These signatures together with many others discussed in Chapter 8 of BSM-SG lead to the following conclusions: (1) The quantum orbits are bound to the individual protons, (2) The neutron is over the proton saddle. Their accumulation also reduces somewhat the strong Coulomb field near the polar regions, (3) the SG field of the protons and neutrons contribute to the energy levels by making the space non-linear. (4) The higher polar axial symmetry is one of the factors that define the nuclear stability, so the most stable isotopes (especially in the lighter elements) contain even numbers of deuterons.

In QED the Lamb shift is explained by a finite nuclear size and vacuum polarization and fluctuation. The latter two phenomena are not clearly defined in Modern Physics, but if the physical vacuum contains some type of medium, the field curvature and all other phenomena of GR are logically explainable. Albert Einstein arrived at this conclusion after he developed General Relativity. In his book *Sidelights on Relativity, page 23* he writes: *To deny Ether is ultimately to assume the empty space is not (with) physical quality. The fundamental facts of (Quantum) Mechanics do not harmonize with this view. According to the General Relativity, space is embodied with physical quality. In this sense, therefore, there exists Ether. According to General Relativity, space without Ether is unthinkable*. [33].

Consequently, we may suggest that in close proximity to a nucleus, a field micro-curvature exists as a GR effect in a microscale range.

2.11. The hidden energy of the physical vacuum as a primary source of the nuclear energy

It is known that the nuclear mass of an element is always smaller than the sum of the masses of protons and neutrons in the atomic nucleus. Such a mass difference, known as mass deficiency or binding energy, is estimated by the Einstein equation $E=mc^2$. The binding energy rises faster at low Z- numbers (especially at He^4) reaching a smooth maximum at Fe and then slowly decreases. The BSM-SG theory provides an explanation for this enigma. The nuclei for lower z – numbers are more compact, while for larger z – numbers they become extended, as shown in Fig. 2. For this reason the SG forces make a more compact field curvature for lower z – number of elements.

A number of observations in Cosmology, such as the flattened rotation curves of the galaxies and the increasing slope of the Hubble plot at large cosmological red-shifts contradict the Big Bang model. In order to solve these problems, a number of theorists suggest the existence of dark energy. According to BSM-SG, the dark energy is a hidden energy existing everywhere in the observable Universe. However, it is not of EM type, but associated with Newton's mass according to the Einstein equation $E = mc^2$. We may estimate this energy by using the revealed material structure of the electron. Using the Einstein equation for the mass of an electron, we obtain

$$E = m_e c^2 = h\nu_c, \quad \text{then} \quad m_e = \frac{h}{c^2}\nu_c \tag{11}$$

where; m_e – mass of electron, h – Planck constant, ν_c - Compton frequency.

Expressing the *m, h, c* and ν_c in Eq. (11) by their dimensions in the SI system we get

$$kg = \frac{Nms}{m^2/s^2}\frac{1}{s} \tag{12}$$

Multiplying Eq. (12) by m^2/m^2 (m – dimension of length) and rearranging we obtain

$$kg = \left(\frac{N}{m^2}\right)\left(\frac{1}{m^2/s^2}\right)\left(m^3\right) \tag{13}$$

This monograph is a result of non-funded theoretical work

The first term on the right side of Eq. (13) is a dimension for pressure, the second is for speed of light (unchanged) and the third one is for volume. Replacing the dimensions by corresponding physical parameters we obtain

$$m_e = \frac{P_S}{c^2} V_e \tag{14}$$

P_S is a kind of static pressure. Since the speed of light is constant we may regard the term P_S / c^2 as a kind of normalized pressure that the space fabric of the physical vacuum exercises on the impenetrable internal volume of the electron. We may estimate it by using the volume V_e of the structure of the electron shown in Fig. 7. It can be expressed as a volume of a torus with a large radius R_c and a small radius r_e. From the oscillating properties of the electron, we see that the ratio between the helical step s_e and the radius r_e can be no less than 2. The dimensionless parameter known as the *g*-factor of the electron determines the electron spin frequency equal to $0.5g\nu_c$ for a free electron in a magnetic field. The g factor is experimentally measured with a high precision $g = 2.002319304$. Its association with the structure of the electron leads to the conclusion that the g-factor is the helical step s_e. This allows us to obtain the small radius $r_e = s_e / g$. Then taking into account that $2\pi R_C = \lambda_C = c/\nu_c$ and s_e given by Eq. (2), the volume of the electron structure is

$$V_e = 2\pi^2 R_C r_e^{\,2} = \frac{\pi\alpha^2 \lambda_C^{\,3}}{g^2(1-\alpha^2)} = 5.96\times10^{-40} \quad (m^3) \tag{15}$$

Solving Eq. (14) for P_S and substituting m_e by Eq. (11) and V_e by expression (15) we obtain

$$P_S = \frac{g^2 ch(1-\alpha^2)}{\pi\alpha^2 \lambda_C^{\,4}} = \frac{g^2 h \nu_c^{\,4}(1-\alpha^2)}{\pi\alpha^2 c^3} = 1.37358\times10^{26} \quad \left[\frac{N}{m^2}\right] \tag{16}$$

Using the Einstein equation $E=mc^2$ and substituting *m* by m_e from by Eq. (14) we obtain

$$E = P_S V_e \tag{17}$$

If the volume V_e is regarded as a reference space volume, the product of static pressure and this volume $P_S V_e$ could also be regarded as a parameter of the physical vacuum. Therefore, according to Eq. (17), this product expresses the energy of the physical vacuum contained in a reference volume $V_e = 5.96\times10^{-40}\,(m^3)$.

$$E = P_S V_e = 8.187\times10^{-14} \quad (J) \tag{18}$$

Expressing this energy for a unit volume of 1 cm^3 we obtain

$$E_S = 1.3736\times10^{20} \quad \left[J/cm^3\right] \equiv 3.18\times10^{13} \quad [KWH] \tag{19}$$

The energy expressed by Eq. (19) is the static energy of the physical vacuum, scaled to a volume of one cubic cm. It looks extremely high but this is because the enormous static pressure P_S is exercised on the extremely small impenetrable volume that the electron and other elementary particles possess. The inter-node distance of the Cosmic Lattice is on the order of $1\times10^{-20}\,(m)$ but the internal lattice of the electron illustrated in Fig. 7 is denser so it is impenetrable. All non-virtual elementary particles contained in the atomic nucleus possess such a dense lattice. One of the densest elements - gold in the solid state - has about 79,170 times lower density. Although the Cosmic Lattice penetrates freely through every body, it does not enter into the denser lattice of the elementary particles. Therefore, we can not detect directly the static pressure P_S. We only feel the effect of acceleration for which the Cosmic Lattice is responsible (this is discussed in Chapter 10 of BSM-SG). So according to BSM-SG theory, the static energy E_S is a hidden energy of the physical vacuum that corresponds to the "dark energy" suggested by some cosmologists.

Consequently, every cubic cm of the physical vacuum space contains a hidden energy of $1.3736\text{x}10^{20}$ (J) equivalent to $3.18\text{x}10^{13}$ (KWH). This, in fact, is the primary source of nuclear energy accessible by the nuclear reactions.

2.12. Access to the hidden space energy by nuclear reaction – an explanation by a General Relativistic effect in the microscale range

The BSM-SG revealed that all stable elementary particles have impenetrable volumes of helical structures like the electron. Their larger mass means that they have larger structures in which the electron structure is just a fractal element. Then **Eq. (14) may serve as a mass equation**. It can be extended to any non-virtual particle by using the volume ratio between that particle and the electron, which is equal to the ratio of their masses. The mass equation is further extended to the nuclear mass of any element given the number of the nucleons (protons and neutrons). In this case it is better to use the ratio between the electron and neutron instead of the proton, since the normal atomic nucleus is neutral. Then the mass of any nucleus can be expressed by Eq. (20)

$$m = \frac{g^2 ch(1-\alpha^2)}{\pi\alpha^2\lambda_C{}^4}\frac{pm_p + nm_n}{m_e} \quad (kg) \qquad (20)$$

where: m_p and m_n – the mass of the proton and neutron respectively, p – number of protons, n – number of neutrons.

The mass equation (20) does not involve the mass deficiency that, according to the Einstein equation $E=mc^2$, provides the binding energy between the nucleons. However, it allows us to infer what is behind the origin of the nuclear forces. According to our hypothesis of the GR effect of field curvature in the space around the nucleus, we may define two zones as in the classical GR effect: a near zone close to the nucleus and a far zone. All our instruments detect the nuclear mass in the far zone. The only parameter that could serve as a scale etalon in Eq. (20) is the Compton wavelength, λ_C, and it is at a power of four. Consequently, it will mostly affect the nuclear mass m. In the near zone, λ_C should be shorter in comparison to our far zone. Similar to detection of the GR gravitational red shift of photons, our instruments will detect lower mass since our reference etalon λ_C (outside of the nuclear field curvature) is larger.

The above analyses lead to two important conclusions: (1) the source of nuclear binding energy is the Static energy of the physical vacuum; (2) the mass deficiency is a result of a GR effect of field micro-curvature around the atomic nucleus;

These conclusions allow us to explain how the nuclear energy is accessible. As in the macro field curvature, the strength of the field curvature around the atomic nucleus depends on the accumulated superdense mass. If the micro-curvature is changed due to fusion or fission, we will get a change in the atomic mass according to Eq. (20), whose equivalent energy is given by the Einstein equation $E=mc^2$. This energy is significant because it is a direct access to the hidden Static energy of the physical vacuum given by Eq. (19). Since these processes in microscale are very fast, the physical vacuum exhibits a stress reaction that causes a depletion or fusion of nuclei and particle and gamma radiation.

Conclusion: The nuclear energy released in the fusion and fission reactions is a result of sudden changes of the GR space micro-curvature around the fused or depleted nuclei.

2.13. Considerations for successful cold fusion

Analysis of successful experiments by using the nuclear models according to the BSM-SG theory unveils the physics of the fusion process in which the Coulomb barrier could be overcome. This leads to the following recommendations.

Considerations:

1. The process of cold fusion is more probable between a heavier and a light nucleus with a proper neutron to proton ratio
2. The knowledge of the real 3D configuration of the nuclei helps to estimate the possibility for deeper penetration of the smaller nucleus into the heavier one. It also allows to find common structural features between elements that showed affinity to cold fusion reactions or transmutations in prior art experiments.
3. The heavier element must be in a solid state in a powder form in order to increase its active surface
4. A proper temperature of the powder substance is required
5. A proper pressure of the light element gas is a prerequisite for the cold fusion process. The applied pressure must also be combined with a pressure pulsation.
6. Optional use of acoustic cavitation in a liquid phase.

This monograph is a result of non-funded theoretical work

7. Optional use of a plasma arc.
8. Optional use of a strong EM pulse

Consideration 1: The smaller nucleus has a shorter range of SG field than a larger nucleus. Then the smaller nucleus in a gas state could more easily get closer to the larger nuclei (as a powder) by applying some momentum via pulsating pressure, an increase of the Brownian motion by temperature, or by ultrasound.

Consideration 2: Heavier nuclei with larger free valences are not recommended since the valence protons (deuterons) have a larger angular freedom and they expand the Coulomb barrier, especially in the ionized state. Elements with smaller valences must be used. They are usually metals.

Consideration: 3. The active surface of a solid state element is increased a thousand times if it is in a micro-powder form.

Consideration 4: The heating increases the Brownian motion of the gaseous component and consequently increases the probability that the lighter nuclei will get closer to the heavier nuclei of the powder. The heavier nuclei may be considered as stationary while their vibrations increase with temperature.

Considerations 5: The constant pressure allows a deeper penetration of the lighter nuclei in the micro-powder, while the pulsating pressure might be helpful for homogenizing the mixture.

Consideration 6: The ultrasound in a liquid phase causes a cavitation with effect of sonoluminescence or even sono-fusion. In fact, it invokes shock waves that may affect the Coulomb barrier (discussed later).

Consideration 7. The plasma arc is a complex process, discussed elsewhere. In some proper plasma excitations, the SG field in proximity to the nucleus is directly affected that may lead to low temperature nuclear reactions. Such reactions, known as nuclear transmutations, have been observed in a number of experiments. Some plasma arc experiments are done in liquids.

Consideration 8. A strong EM pulse invokes a shock wave in the operative medium. At the boundary between the solid and gas phase the shock wave causes a stress in which the SG forces modify the Coulomb barrier.

3. Analysis of some cold fusion experiments by using the BSM-SG models of atomic nuclear structures

Using the BSM-SG models of atomic nuclei one may obtain not quantitative but a qualitative estimate of the feasibility of selected cold fusion processes. They will help to do:

1. A proper selection of the elements to be involved in the nuclear fusion, and the shape of the involved gas molecule (more specifically for hydrogen)
2. Selection of proper environment and technical method
3. Overcoming the Coulomb barrier by proper orientation of the Coulomb field of the proton (deuteron) in respect to the 3D structure of the heavier atomic nucleus at the moment preceding fusion

The last consideration could be achieved by dynamic confinement using properly configured magnetic fields, but this might be more appropriate for experiments than for nuclear energy.

3.1 Theoretical considerations about using the BSM-SG models of the atomic nuclear structures

The BSM-SG models for the most abundant isotopes of the elements of the Periodic Table for $1 \le Z \le 103$ (Z – number of protons) are given in the Atlas of Atomic Nuclear Structures (ANS) [17]. It is included as an appendix to the BSM-SG book [16,24] and was also published elsewhere. Detailed description of the nuclear structures and how the nucleons are connected by different bonds is provided in Chapter 8 of the BSM-SG book. The ANS contains a short introduction, Part 1, Part II and a Periodic table poster in which the atomic nuclei are arrange in the same way as in the Classical Periodic Table of elements. Part I (page 1-1 to page 1-4) shows the structure of the stable elementary particles: electron, proton and neutron with their physical dimensions and the nuclei of the simplest elements: Hydrogen, Deuterium and Helium. Part II (pages II-0 to II-20) shows the arrangement of nucleons (protons and neutrons) in the atomic nuclei for the stable isotopes of elements from Hydrogen to Lawrencium. The protons and neutrons comprising the atomic nuclei are connected by different types of bonds, as they are described in Chapter 8 of BSM-SG. In order to simplify the drawings in the Atlas of ANS, the shapes of protons and neutrons are drawn by symbols – an arrow for the proton and a cross-line for the neutron. The different bonds are also shown by symbols. In page II-0 the symbols for the proton, the neutron and their bond connections are shown. In part II the nuclear structure of all elements are shown by two graphical views using the symbols. They show all the features of the real 3D nuclear structure of the elements, with the exception of its

This monograph is a result of non-funded theoretical work

slight twisting. The latter feature is a result of the real shape of the proton that is not a flat curve but a 3D curve obtained by twisting a torus to a shape close to a figure 8. The electron orbits are not shown but they are easily identifiable, since their trajectory is defined by the close proximity shape of the proton's electrical field. For a clearer visualization of the nuclear shape, some selected atomic nuclei are shown on page II-21 in the Appendix ANS of BSM-SG book and Fig. 2 of this article. In this visualization, the nuclei are shown by a polar view and polar section. In the polar section, only protons and neutrons closer to the section are shown. For any atom, a 3D mockup from 0-ring springs twisted and folded as the shape of the proton and neutron. They provide a good 3D vision about the nuclear configuration, bond connections, orbitals and valences of the atom. This is illustrated in the US Patent obtained by the author [34]. It could be used also for better understanding of the nuclear interactions in cold fusion research or nuclear chain reactions. Alternatively, this could be realized by rotating computer graphics.

3.2. Analysis of cold fusion experiments based on acoustic cavitation or strong EM pulse

One of the earliest researchers on cold fusion is Hugh. G Flyn (1913-1997), a former professor at the University of Rochester and an internationally recognized expert on ultrasonic waves in liquids. When properly applied, the ultrasonic waves cause an effect known as cavitation that invokes shock waves by the collapse of gas bubbles in liquids. In 1978 he applied for a patent "Method of Generating Energy by Acoustically Induced Cavitation Fusion and Reactor Therefore", granted in 1982 [1]. He advises using the ultrasonic method for generating a bubble in a liquid metal or alloy injected with hydrogen isotopes (hydrogen or deuterium or tritium), and the application of a positive pressure on the bubble to accelerate the adiabatic stage which causes the bubble to contract to a smaller radius, thus increasing the maximum temperature and pressure within the bubble. At or near its minimum radius, the bubble generates a very intense shock wave. This causes hydrogen isotopes injected in the metal liquid to undergo thermonuclear reactions. The patent contains a detailed discussion on properly selected metals and alloys, the operational parameters and the reactor design. One of the optimal choices for obtaining an energy output on the order of 200 KW is to use Li at a temperature of 1000K to 1200K (727C to 927C) in which a fusion of deuterium will start from the beginning. Flyn claimed that the proposed method creates a number of H – isotopes including Tritium and even Helium. One of the most energetic nuclear reactions claimed by Flyn is

$$ {}_1H^1 + {}_3Li^7 = 2\,{}_2H^4 + 17.35MeV \qquad (21) $$

The cold fusion theorist and Nobel Laureate Julian Schwinger in his talk at MIT on November 11, 1991 emphasized the cavitation method of cold fusion and associated it with a coherent sonoluminescence [5]. Mentioning the formation of tritium and helium, Flyn Schwinger says: "*When I first heard about coherent SL (sono-luminescence), some months ago, my immediate reaction was: "This is a dynamical Casimir effect*". His statement is in full agreement with the BSM-SG concept, according to which the Casimir forces are a signature of the SG forces. They are able to modify the Coulomb field in a micro scale range at the boundary of the collapsing bubbles.

Recently the cavitation method was brought to attention by some groups, and in 2006 R. P. Taleyarkhan and colleagues from Purdue University published an article in PRL about a laboratory sono-fusion experiment that invoked nuclear reactions by cavitation in a cell containing a deuterated benzene and acetone mixture. They claimed detecting emission of neutrons with energy ≤2.45 MeV, which is indicative of a fusion reaction. When using only a deuterium liquid, such an emission was not observed. The results invoked a hot debate with some accusations of falsified results after one replication attempt by UCLA researchers B. Naranjo and S. Puttermandid not provide the same results. The on-line article of Taleyarkhan et al. in PRL was removed (only the abstract is left), but they published a more extensive article in Nuclear Engineering and Design [35], naming the experiment as 'acoustic cavitation bubble fusion". In fact B. Naranjo and S. Putterman are competitors in the race for cold fusion based on their method of nuclear fusion driven by a piezoelectric crystal, in which the Coulomb barrier is modified. In their article in Nature they claim that an electrostatic field of the crystal is used to generate and accelerate a deuteron beam (> 100 keV and >4 nA), which, upon striking a deuterated target, produces a neutron flux over 400 times the background level [36]. They do not provide a physical explanation, but cite alternative approaches, such as inertial confinement, Coulomb explosions of deuterium clusters, and ultra-fast laser–plasma interactions. The experiments of Taleyarkhan et al. and B. Naranjo and S. Putterman may not lead to a practical method for obtaining energy, but they possess the measurable feature of fusion products.

This monograph is a result of non-funded theoretical work

Some cold fusion researchers claim that they obtained fission products by applying a strong EM pulse in a plasma environment. One of the prominent scientists and researchers using a plasma method for cold fusion is Ruggero M. Santilli [31]. He developed a method he named "spin coupling" as a pre-conditioning for cold fusion. The preconditioned gas he called magnegas and the atoms – magnecules. Santilli built hadronic generators in which he used carbon and conveyed hydrogen or deuterium gas under pressure, and an electrical arc (plasma). He claimed that he observed excess heat from a fusion reaction (C+D -> N + energy). He says that the energy yield is larger if the gas is preconditioned as a "magnegas". According to BSM-SG, the Santilli magnecule of Hydrogen corresponds to the ortho-state of the hydrogen molecule illustrated in Fig. 8.a. In a normal hydrogen gas, the molecules in such a state are a small percentage. The other para-state (Fig. 8.b) is more abundant since the molecular binding is stronger so it is more resistant to collision depletion due to Brownian motion. The application of plasma discharge may convert the para to the ortho–state. The two protons in H_2 ortho-state (Fig. 8. a.) (or deuterons for D_2 ortho-state) have an orientation similar to the two deuterons in the atomic nucleus of Gd, (Fig. 6.) that fuse into a He nucleus (alpha particle) at room temperature. Consequently, the ortho-state of the H_2, and especially the D_2 molecule, is more promising for cold fusion. This is illustrated in the next sections.

According to BSM-SG, a shock wave is created in both methods - the cavitation bubble fusion and the strong EM pulse in plasma. It involves stress at the boundary between the atoms of heavier and lighter elements. In such stress, the SG forces are directly accessed causing modification of the Coulomb barrier. In this process, some reactive energy could also be borrowed from the Static energy of the physical vacuum.

Fig. 12 illustrates graphically (by using the BSM-SG atomic models) some of the reactions claimed by Flyn and the group of Taleyarkham, including the reaction shown by Eq. (21).

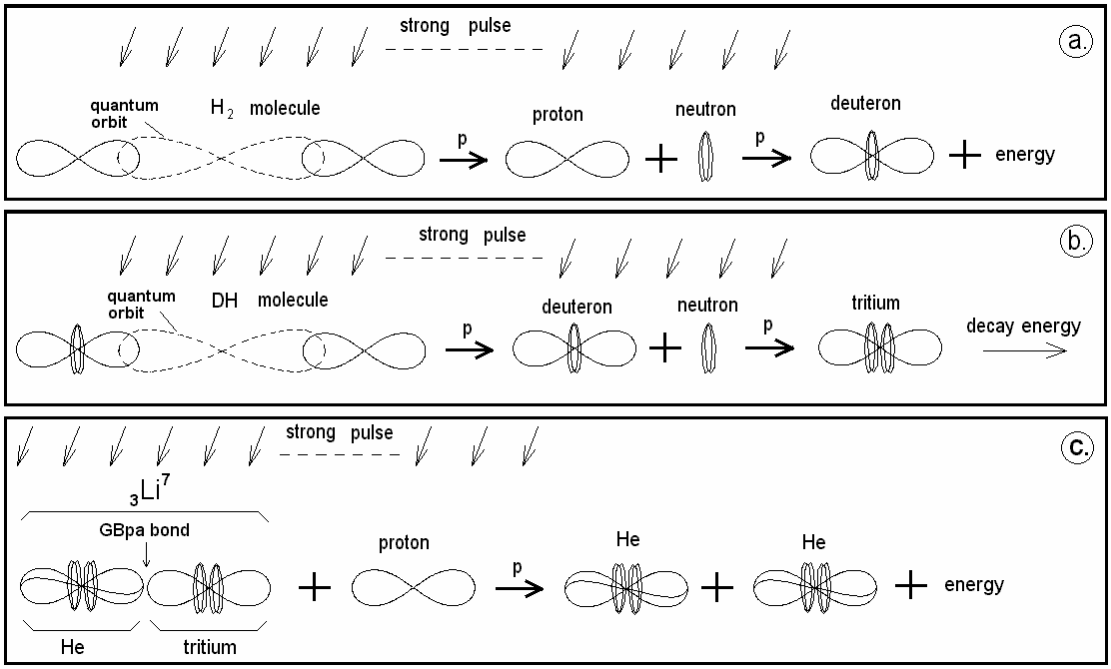

Fig. 12. Cold fusion by strong shock pulse in sono-fusion or EM pulse in plasma (a) H2 -> p + n -> D; (b) HD -> D + n -> T, (c) L + p -> 2 He . The $_3Li^7$ nucleus is comprised of He and T nuclei attached by GBpa bonds (§8.3.6, Chapter 8 of BSM-SG). The arrow symbol with p denotes a probability for the nuclear reaction. The He nucleus is shown by the symbol used in ANS.

In fact, the strong pulse could be either from an acoustic cavitation or from a strong EM pulse in plasma. The working environments for both methods are different but they may invoke the same nuclear reactions (a) and (b) illustrated in Fig. 12. By using the BSM-SG models, all nuclear reactions suggested by Flyn in his patent can be illustrated.

Now let us focus on experiments based on Palladium and Deuterium in which a change of the natural isotope ratio Ag/Pd is observed. This means that a nuclear reaction Pd + D -> Ag takes place. Such results have been reported by Dash, J. and S. Miguet in 1996 [37]. The symbolic graphics of the nuclear structures of Pd and

Ag are shown in pages II-9 and II-10 of the ANS Appendix A in BSM-SG book [24] and elsewhere [17]. The two views made from the symbolic graphics are shown in Fig. 13 together with the atomic nucleus of deuterium. The nuclear size dimensions are based on the dimensions of the proton, obtained in BSM-SG. The nuclear Coulomb barrier shown by a gray color is for illustration only (not based on calculations).

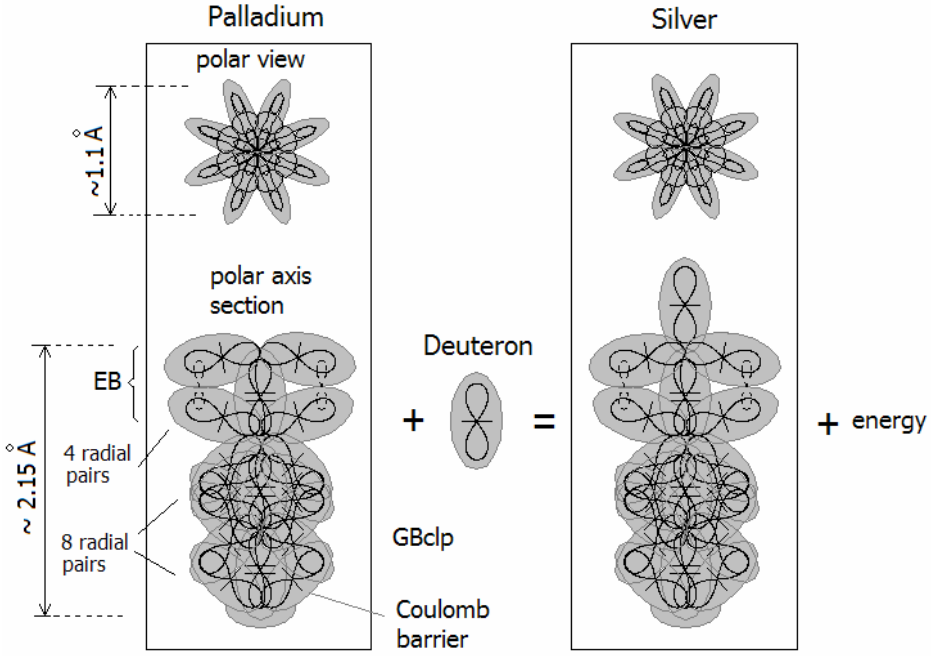

Fig. 13. Illustration of Pd+ D -> Ag reaction. The Coulomb barrier is shown by a gray color.

It is apparent that a single deuteron is probably fused in the upper polar region of Pd converting it to Ag. What is the reason for expecting this to occur at the top pole? The answer will come from examining the trend of the atomic nuclear build-up with the z-number increase. The top pole contains four radial pairs of EB bonded deuterons, while the bottom pole contains 8 pairs of GBclp bonded deuterons. The upper Coulomb barrier at the top pole is more rarefied and the single deuteron may penetrate closer.

The four pairs of deuterons are connected by quantum orbits, so they are called Electronic Bonds (EB). The EB bonds are excluded from the principal valence, but they could be broken in some strong chemical reagents. The single deuteron at the top pole in silver defines the principal valence. Or, it could be a proton only. The GBclp (close proximity gravitational bonds) are superstrong since they are held by SG forces. These bonds make the completion of the shells of noble gases and they are completely excluded from any valence. The middle section of the nuclear chain also contains 8 radial pairs of GBclp but they are slightly squeezed by the SG forces to make the nucleus more compact (this becomes clearer when the whole 3D nuclear structure is rotated). The middle and bottom region of 16 deuterons corresponds to the completed internal shell of the electrons according to the QM models. Some pairs can be from tritium nuclei.

In the hot fission or fusion experiments, the nuclear reaction is always accompanied by radioactivity and especially alpha radiation. The alpha particles are helium nuclei. One of the objections against cold fusion was that helium is not detected, but this is not true. Dr. Les Case from New Hampshire is one of the first who detected helium using palladium as a catalyst in a deuterium atmosphere [13]. The phenomenon, called “Case effect”, has been confirmed by other researchers [38]. The palladium in this case of nuclear reaction, the palladium plays the role of a catalyst. The process is illustrated in Fig. 14 by using the BSM-SG nuclear models.

The deuterium molecule D_2 in its most common state is similar to the H_2 molecule shown in Fig. 8.a. (analysis for the D_2 molecule similar to that for the H_2 molecule is made in §9.8, Chapter 9 of BSM-SG). In order to fuse to helium, the following two conditions are necessary: (1) the two deuterons must get much closer, while keeping the axial orientation (as in the case of deuterons preceding the alpha decay in Gd, shown in Fig 6), (2) the Coulomb barrier of the proton shown in Fig. 4 must be temporarily disturbed. These conditions could be fulfilled if the D_2 molecule is pushed and temporarily trapped between the 4 deuteron pairs at the upper pole region of the Pd nucleus. At room temperature and normal pressure, such a process has a low probability. However, if applying Considerations 3, 4, and 5, the probability may increase, leading also to an increase of the energy yield.

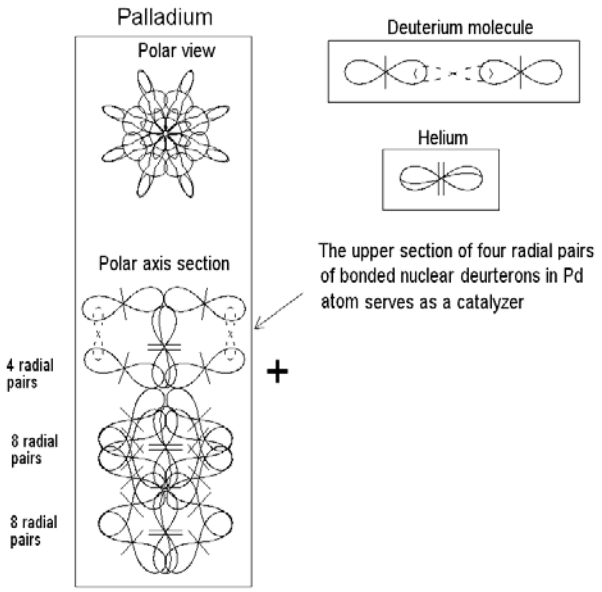

Fig. 14. The role of Palladium as a catalyst for D+D -> He nuclear reaction, from the point of view of the BSM-Supergravitation Unified theory

3.3 Italian cold fusion research. Piantelli and Focardi-Rossi methods.

The research on cold fusion in Italy was initiated at the end of 1989 by Francesco Piantelli, a professor at the University of Sienna, now retired. The research began with observing a strange thermal effect at low temperature in a sample of nickel in hydrogen atmosphere. Piantelli has a few patents and publications [8]. He designed reactors and did extensive research on different elements in hydrogen and deuterium atmosphere and obtained fusion byproducts and energy release [39]**.** He used mostly rods coated with the selected elements by special technology. The problems for successful commercialization have been of technical issue: the operating temperature was still high in the order of 2000^0C, the reactor was under pressure about 0.5 bar and the reaction was not very stable [39]. The research of Piantelli was extended and supported by the local inter-university centers from Bologna (Focardi, Campari) and Sienna (Piantelli, Gabbani, Montalbano, Veronesi). A detailed report about this research is published by the Italian National Agency for New Technology, Energy and Environment in 2008 [9]. Recently, Piantelli created a company. The nuclear process suggested by Pinatelli is Ni + H -> Cu or Ni + D -> Cu.

Fig. 15 illustrates the nuclear reaction Ni + D-> Cu by using the BSM-SG models.

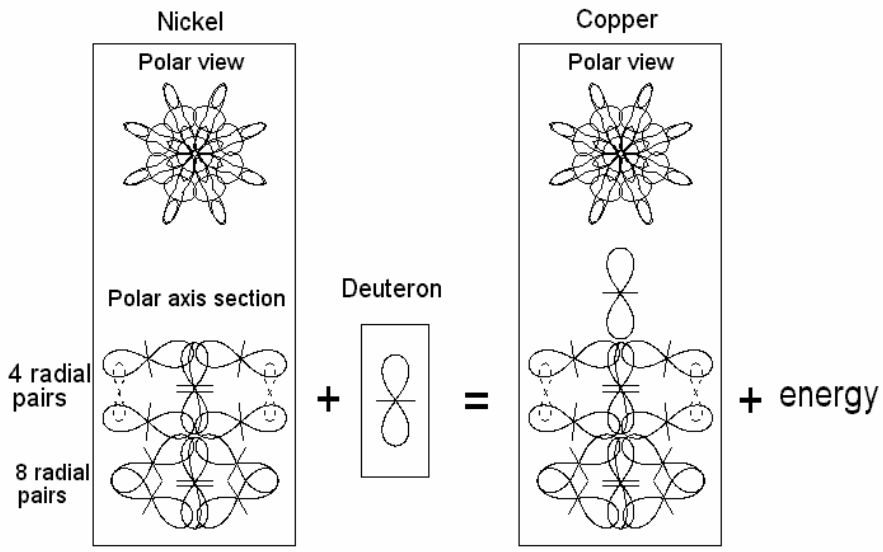

Fig. 15. The nuclear reaction Ni + D -> Cu illustrated by BSM-SG models

This monograph is a result of non-funded theoretical work

Comparing the atomic nucleus of Ni (Fig. 15) with the nucleus of Pd (Fig. 14) we see one striking similarity despite the different atomic mass. The upper polar regions for both nuclei contain 4 radial pairs of Deuterons. Consequently the nuclear reaction Ni + D -> Cu becomes similar to the nuclear reaction Pd + D -> Ag.

The method of Piantelli has been further elaborated by the cooperative work between Sergio Focardi, an emeritus professor at the University of Bologna and Andrea Rossi, an inventor and entrepreneur. This led to the successful development of a method for cold fusion based on the fusion reaction Ni + H -> Cu, with a significant energy output. Andrea Rossi filed a patent application on April 9, 2008 [12]. It includes the following abstract.

A method and apparatus carrying out highly efficient exothermal reaction between nickel and hydrogen atoms in a tube, preferably, though not necessary, a metal tube filled by a nickel powder and heated to a high temperature, preferably, though not necessary, from 150 to 5000C are herein disclosed. In the inventive apparatus, hydrogen is injected into the metal tube containing highly pressurized nickel powder having a pressure, preferably though not necessary, from 2 to 20 bars.

At the end of the year 2010, A. Rossi had a working prototype for demonstration and claimed that he had manufactured a few cold fusion reactors. On January 14, 2011, Rossi and Focardi gave the first public demonstration announcing that the reactor called E-cat is capable of producing more than 10 kilowatts of heat power, while only consuming a fraction of that. During the year 2011, five additional demonstrations and tests were provided with some invited scientists from universities. Rossi claimed that he had achieved an output/input average energy ratio of 200. On October 28, 2011, a large public demonstration took place at the University of Bologna, Italy, where Rossi demonstrated 1 MW system comprised of parallel E-cat reactors. The reactors worked in a self-sustained mode releasing heat that was used to turn water into steam. According to Rossi, each reactor produced an average of 470 kilowatts of heat for more than five hours, so the total obtained energy was 2635 KWH. On November 11, 2011, Rossi announced that in one year's time he will demonstrate a cold fusion reactor with an electrical output.

According to our analysis, the major success of the Focardi-Rossi and Rossi invention is due to the following improvements over the prior art. The first one is that Nickel is in the form of powder with an average granular size of about 10 um, obtained via some private technology. The second one is that a pulsing pressure is superimposed on a highly pressurized hydrogen gas. The major achievement is in lowering the working temperature below 500^0 C. According to Rossi, he also uses a catalyzer based on a small number of elements. This issue is a subject of on-line comments, but it may not be so important since Piantelli now claims that he obtained satisfactory results without a catalyzer. The first improvement introduced by Rossi vastly increases the surface area of Ni, according to our consideration 3, while the second improvement is according to our consideration 5. The other considerations 1 and 4 are also applied in the E-cat reactor, while consideration 2 might have been intuitively guessed by Piantelli since Nickel is in the same vertical group as Palladium. Some public reports mentioned that an RF generator was used, but our vision is that it might only have helped to initiate the cold fusion reaction. Also, it may not be a standard RF generator, but a generator providing a burst of frequencies with a broader spectral range, which may cause micro plasma effects (sparks) in the Nickel powder. This is in agreement with our consideration 7 or 8. Rossi also mentioned that he obtained successful results when using the isotopes Ni^{62} and Ni^{64} (34 and 36 neutrons respectively), where the number of protons in Ni are 28. The reactions are Ni^{62} +H->Cu^{63} and Ni^{64} +H->$Cu^{65.}$ According to BSM-SG, for the stable isotopes of Ni with a larger and even number of neutrons, the four pairs in the upper polar region are more likely deuterons or even tritium rather than protons. The Coulomb barriers in the case of deuterons or tritium pairs are more compact, allowing closer penetration of the proton or deuteron from the gas. The tritium nuclei, although stable, could be made to decay more easily, by releasing a neutron. In this case some fission reactions may occur but they may not lead to so much radioactive byproducts like from the heavier elements like uranium. This may explain the small amounts of lighter elements detected (such as sulfur, chloride, potassium, calcium) after operation of the reactor. According to Rossi and the presented mass spectroscopy charts in Fig. 3 and 4 in his patent [12], we see clear peaks of Cu and Zn (mentioned also in the patent text). These elements, which were not initially contained in the nickel powder, are the main product of the cold fusion reactions contributing to the released energy.

Fig. 16. illustrates the nuclear structures of Ni, Cu and Zn.

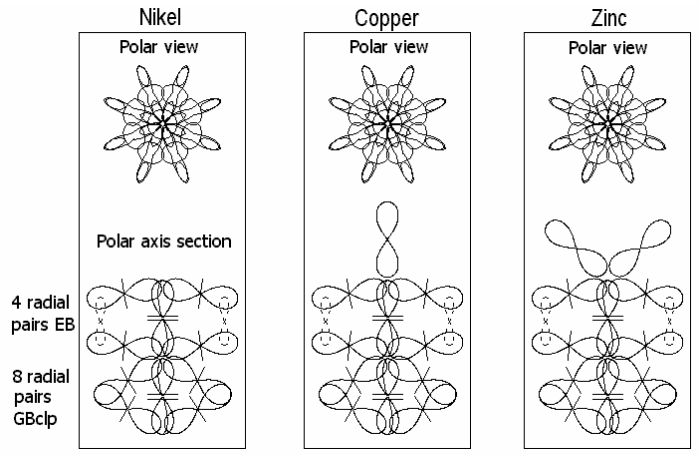

Fig. 16. Ni, Cu and Zi nuclei. Ni nucleus is embedded unchanged in Cu and Zn nuclei. The single unbound proton in Cu and the two unbound protons in Zn define their principal valence.

The single principal valence of Cu is due to the single proton in the upper pole, while in Zn it is from two protons. Ii is expected that if deuterium gas were used instead of hydrogen, the principal valences of Cu and Zn would be from deuterons and the reaction could be even more efficient. It is also apparent that the H_2 or D_2 gas must be in the ortho state. For initiating the nuclear process at a lower temperature, the conversion of para to ortho-state may be triggered by an RF generator burst, but after that it would be supported by the heat or a small amount of X or gamma radiation. It is also apparent that the nickel nucleus becomes embedded in copper and zinc without any refurbishing, that explains a lack or insignificant amount of particle radiation. The small amount of such radiation will be mostly caused by some neutrons that escaped from the upper 4 pairs if some of them are from tritium nuclei. If cached in improper place by some Ni nuclei they will cause fission reaction but with much less the fission byproducts in comparison to the uranium fission chain reaction.

It is worth noting that, based on our analysis of the successful cold fusion processes and particularly those of the Italian researchers, we conclude that another option of cold fusion based on Cr instead of Ni could be also feasible.. The chromium nucleus has a similar arrangement as nickel with only difference that it has a 2 radial pairs with EB bonds in the upper polar region instead of 4 at nickel. This signature is apparent from the similarity between the Lamb shift patterns of the group of Cr, Mn and Fe and the group of Ni, Cu, and Zn shown in Fig 11. b. and from many other considerations discussed in Chapter 8 of BSM-SG. The expected reaction is Cr + H -> Mn or Cr +D -> Mn while some probability for additional reaction leading to Fe also exists.
We recommend using the stable isotope Cr^{54}, the D_2 gas in ortho-state and observing the considerations listed in section 2.13. Fig. 17. illustrates the nuclei of Cr, Mn and Fe using the BSM-SG models.

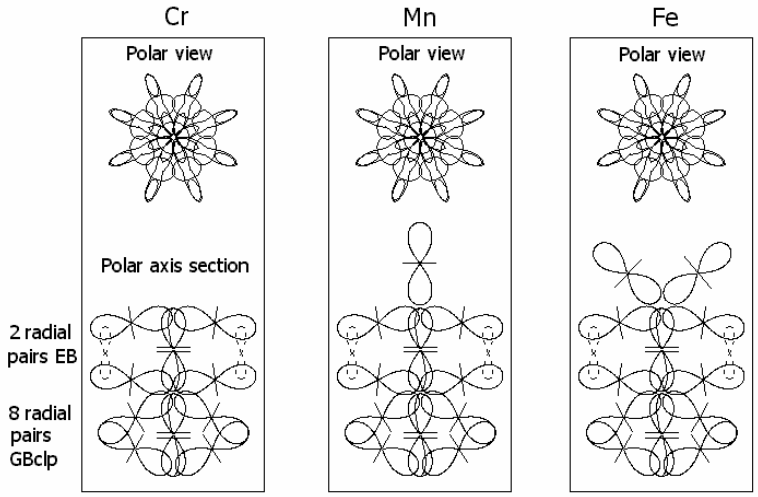

Fig. 17. Cr, Mn and Fe nuclei according to the BSM-SG nuclear models

4. Discussions and conclusions:

The BSM-SG models of atomic nuclei presented in the Atlas of Atomic Nuclear Structures (ANS) provide a new vision about nuclear reactions and, more particularly, the feasibility of cold fusion. The Coulomb field below the Bohr radius does not converge to a sphere with a radius of about 1 x 10^{-15} (m) and it is also not spherical. So the Coulomb barrier of the proton does not rise to a very high strength. The Coulomb barrier of the atomic nucleus is formed from superimposed Coulomb barriers of the protons as illustrated in Fig. 13. The shape of the nuclear Coulomb barrier might be slightly modified from the neighboring atoms in solids and especially in a metal lattice. It could also be affected by some technical methods that cause a stress. This may lead to successful cold fusion between properly selected elements if using the methods discussed in section 2.13. The nuclear structures presented in the ANS provide information for selection of the involved elements. From the point of view of the BSM-SG nuclear models, the lack of radioactive byproducts and the insignificant amount of radioactivity in cold fusion experiments is reasonable. Why is this? A careful examination of the BSM-SG models in ANS reveals that when the neutrons are symmetrically distributed in the atomic nucleus, the corresponding isotope is stable. In the case of cold fusion there is not a severe disturbance of the nuclei that lead to refurbishing of the stable isotopes with the release of neutrons and alpha particles. In hot fusion and fission chain reactions the conditions are quite different. In hot fusion, the atomic nuclei are subject to superstrong collisions leading to refurbishing of the nuclei, so even in the case of low atomic mass nuclei, a significant release of neutrons, gamma and beta radiation takes place. In the nuclear fission chain reactions, heavy nuclei are involved and when a slow neutron is trapped in the nucleus, it is usually not in the right place. The nuclear symmetry is severely disturbed and the process of decay and nuclear refurbishing follows immediately, releasing a large amount of unstable nuclei, neutrons, alpha particles, and beta and gamma radiation. Such a violent process could not take place in cold fusion or nuclear transmutation. The major advantages of cold fusion are the smooth release of energy and the lack of radioactive byproducts or strong radioactivity. Consequently, cold fusion should be a very safe replacement for the nuclear energy based on fission chain reaction or hot fusion. These are big advantages contributing to safety and lack of hazardous radioactive waste.

Today when the safety of nuclear energy is a big concern after the nuclear catastrophes in Chernobyl and Fukushima, the search for a safer alternative is more important than ever before. The radioactive waste from all nuclear plants in the world grows by 12,000 metric tons per year. By the year 2015, it will reach about 250,000 tons. According to a study by Los Alamos National Laboratory, a microgram of Plutonium entering the human body through the food chain will cause a fatal illness leading to cancer in 10 years [40].

Acknowledgements

I would like to express my special thanks to Acad. Dr. Asparuh Petrakiev for the organized seminars, summer conferences and useful discussions. I appreciate the discussions with William Treurniet and his help in the editing of English version of this monograph.

References:

[1] Hugh G. Flyn, Method of generating energy by acoustically induced cavitation fusion and reactor therefore, US Patent 4,333,796 (filed 1978, issued 1982)
[2]. M. Fleischmann and S. J. Pons, Electroanal. Chem, **261**, 301, (1989)
[3] E. F. Mallove, Ninth International Conference on Cold Fusion (ICCF9) Meets in Beijing, China, www.infinite-energy.com/iemagazine/issue44/iccf9.html
[4] http://www.lenr-canr.org/ Low energy nuclear reaction (LENR) or cold fusion. Website containing a library of more than 1,000 scientific papers reprinted with permission from the authors and publishers.
[5] J. Schwinger, A progress Report: Energy Transfer in Cold Fusion and Sonoluminecsence, Infinite Energy, Issue 24, p. 19, (1999)
[6] http://www.tcm.phy.cam.ac.uk/~bdj10/ (B. Josephson web page), http://www.youtube.com/watch?v=EDv6phew-ck
[7] T. O. Parssell, Pd-110/Pd108 Ratios and Trace Element Changes in Particulate Palladium Exposed to Deuterium Gas, Tenth Int. Conf on Cold Fusion, 2003, CambridgeMA:LENR-CANR.org
[8] F. Piantelli, http://www.rexresearch.com/piantelli/piantelli.htm
[9] Cold Fusion. The history of research in Italy. Italian National Agency for New Technologies, Energy and Environment,

This monograph is a result of non-funded theoretical work

Report in, 2008. Editors S. Martelluci, A. Rosati, F. Scaramuzzi, V. Violante

[10]. S. Focardi and A. Rossi, http://www.journal-of-nuclear-physics.com/?p=360
[11] S. Focardi et al., Large excess heat production in Ni-h system, IL Nuovo Cimento, v. 111 A, N.11, 1233-1242, (1998)
[12] A. Rossi, Method and Apparatus for Carying out Niclkel and Hydrogen Exothermal Reactions, WO 2009/125444 A1 (15 Oct 2009) (patent submitted 4 Aug 2008).
[13] http://www.infinite-energy.com/iemagazine/issue25/deviceupdate.html
[14] Tadahiko Mizuno, Experimental Confirmation of the Nuclear Reaction at Low Energy Caused by Electrolysis in the Electrolyte, Proceedings for the Symposium on Advanced Research in Energy Technology 2000, Hokkaido University, March 15, 16 and 17, 2000, pp. 95-106
[15] S.Sarg. Helical Structures Forum http://www.helical-structures.org (launched on 17 Oct 2011)
[16] S. Sarg ©2001, *Basic Structures of Matter*, monograph, http://www.helical-structures.org also in: http://www.nlc-bnc.ca/amicus/index-e.html (First edition, ISBN 0973051507, 2002; Second edition, ISBN 0973051558, 2005), (AMICUS No. 27105955), LC Class no.: QC794.6*; Dewey: 530.14/2 21
[17] S. Sarg © 2001, Atlas of Atomic Nuclear Structures, ISBN 0973051515, http://www.nlc-bnc.ca/amicus/index-e.html (April, 2002), (AMICUS No. 27106037); Canadiana: 2002007655X, LC Class: QC794.6*; Dewey: 530.14/2 21 (also http://vixra.org/abs/1107.0031)
[18] S. Sarg, *New vision about a controllable fusion reaction*, monograph, www.nlc-bnc.ca/amicus/index-e.html (ISBN 0973051523, April, 2002), (AMICUS No. 27276360); Canadiana: 20020075960
[19] S. Sarg, New approach for building of unified theory, http://lanl.arxiv.org/abs/physics/0205052 (May 2002)
[20] S. Sarg, A Physical Model of the Electron according to the Basic Structures of Matter Hypothesis, Physics Essays, vol. 16 No. 2, 180-195, (2003)
[21] S. Sarg, Basic Structures of Matter Theory and Derived Atomic Models (2002)Journal of theoretics http://www.journaloftheoretics.com/Links/Papers/Sarg.pdf
[22] S. Sarg, BSM - Supergravitation unified theory based on an alternative concept of the physical vacuum, Proceedings of the IX International Scientific Conference "Matter, Energy, Gravitation", 7-11 Aug 2006, St. Petersburg, Russia.
[23] S. Sarg, Basic Structures of Matter – Supergravitation Unified Theory based on an Alternative Concept of the Physical Vacuum, Poc. Of Natural Phylosophy Alliance, 17th Annual Conference 23-26 July, 2010 at California State University, Long Beaches, CA
[24] Stoyan Sarg, ***Basic Structures of Matter –Supergravitation Unified Theory***, Trafford Publishing, 2006, ISBN 1412083877
[25] Ph. M. Kanarev, and Tadahiko Mizuno, COLD FUSION BY PLASMA ELECTROLYSIS OF WATER, http://guns.connect.fi/innoplaza/energy/story/Kanarev/coldfusion/index.html
[26] Ph. M. Kanarev, Models of the Atomic Nuclei, http://www.journaloftheoretics.com/Links/Papers/Kanarev-Atomic.pdf Image of carbon sheet, Popular Science, (01.19.2010) www.popsci.com/gadgets/article/2010-01/graphene-breakthrough-could-usher-future-electronics
[27] A. Javey at al., Nano Lett. **4**, 1319, (2004) (single wall nanotube)
[28] Image of carbon sheet, Popular Science, (01.19.2010) www.popsci.com/gadgets/article/2010-01/graphene-breakthrough-could-usher-future-electronics
[29] J. E. Polard et al, Journal of Chemical Physics, **77**, 34-46 (1982) (PE spectra)
[30] I. Dabrowsky, Canadian Journal of Physics, **62**, 1639 - (1984) (H2 optical spectra)
[31] R. Santilli http://santilli-foundation.org/
[32] G. W. Erickson, Energy Levels of One-Eelectron Atoms, Phys. Chem. Ref. Data, V.6, No. 3, (1977)
[33] A. Einstein, *Sidelights on Relativity*, translated by: G. B. Jeffery and W. Perret, Methuen & Co. London, (1922); republished unabridged and unaltered: Dover, New York, (1983)
[34] S. Sargoytchev, US Patent US D439,198 S, submitted on June 23, 1999, issued on March 20, 2001.
[35] R. P. Taleyarkhan et al., Modeling, analysis and prediction of neutron emission spectra from acoustic avitation bubble fusion experiments, Nuclear Engineering and Design, 238, 2779-27-91 (2008)
[36] B. Naranjo J.K. Gimzewski & S. Putterman, Observation of nuclear fusion driven by a pyroelectric crystal, Nature, 434, 1115-1117 (2005)
[37] Dash, J. and S. Miguet, *Microanalysis of Pd Cathodes after Electrolysis in Aqueous Acids.* J. New Energy, 1996. **1**(1): p. 23
[38] http://pages.csam.montclair.edu/~kowalski/cf/47catalytic.html (About Case effect)
[39] Francesco Piantelly, Energy generation and generator by means of anharmonic stimulated fusion, Patent WO 9520816, (1997).
[40] Voelz, George L. "Plutonium and Health: How great is the risk?". *Los Alamos Science* (Los Alamos (NM): Los Alamos National Laboratory) (26): 78–79, (2000)

This monograph is a result of non-funded theoretical work